

ALMA MATER STUDIORUM - UNIVERSITÀ DI BOLOGNA

SCHOOL OF ENGINEERING AND ARCHITECTURE

Department of Electrical, Electronic and Information Engineering

"Guglielmo Marconi" - DEI

Master Degree in Telecommunication Engineering

Master Thesis

in

Technologies and Applications of Wireless Power Transfer

**BATTERY-LESS SOLUTIONS ENABLING
LORA TRACKING IN INDUSTRIAL PLANTS**

Supervisor

Prof. Alessandra Costanzo

Presented by

Ahmet Barış Gök

Co-Supervisors

Prof. Diego Masotti

Ing. Francesca Benassi

Academic Year 2020/2021

Call II

Contents

| | | |
|----------|--------------------------------|-----------|
| 1 | Introduction | 4 |
| 2 | LoRa Module | 12 |
| 3 | Antenna Design | 17 |
| 3.1 | Monopole Array | 19 |
| 3.2 | Patch Array | 26 |
| 4 | Circuitry Design | 31 |
| 4.1 | Power Splitter | 31 |
| 4.2 | Rectifier | 34 |
| 4.3 | Coaxial Cable | 38 |
| 5 | Power Budget Evaluation | 40 |
| 6 | Conclusion | 43 |
| 7 | Future Work | 45 |
| 8 | Bibliography | 46 |

1 Introduction

According to [1], by 2050, passenger demand for mobility will increase by 200-300% and freight activity by 150-250%, which means that smart solutions are required to be implemented to provide suitable transport capacity for continuously growing volumes of goods and people. Speed and access to data will influence customers' relationship to transportation, and also their decision making processes, since they will await reliable and accurate real-time information, and consider optimal pricing for the services. Customer-centric products and services will be based on information about the individual passengers and their needs. Smart Mobility is therefore only one of the topics regarding the Smart City implementation, improving on the quality of life of citizens [2].

Smart Mobility basically includes systems that are used to provide seamless, efficient and flexible travel across all modes of transport. This is illustrated in Figure 1 which shows a number of elements which make up smart mobility including operational and strategic modelling, instrumented smart infrastructure and intelligent transport systems. In practice, this would translate into smarter connected vehicles, trains and public transport systems which would increasingly sense their surrounding environments and improve safety in situations where driver mistake is the most common. For instance, a range of GPS, on-board public transport, video surveillance, position fixing, and communications equipment are increasingly providing more accurate and trustworthy multi-modal real-time passenger information, which results in better informed travellers and ensuring a safer, smoother and more reliable experience for the users [3].

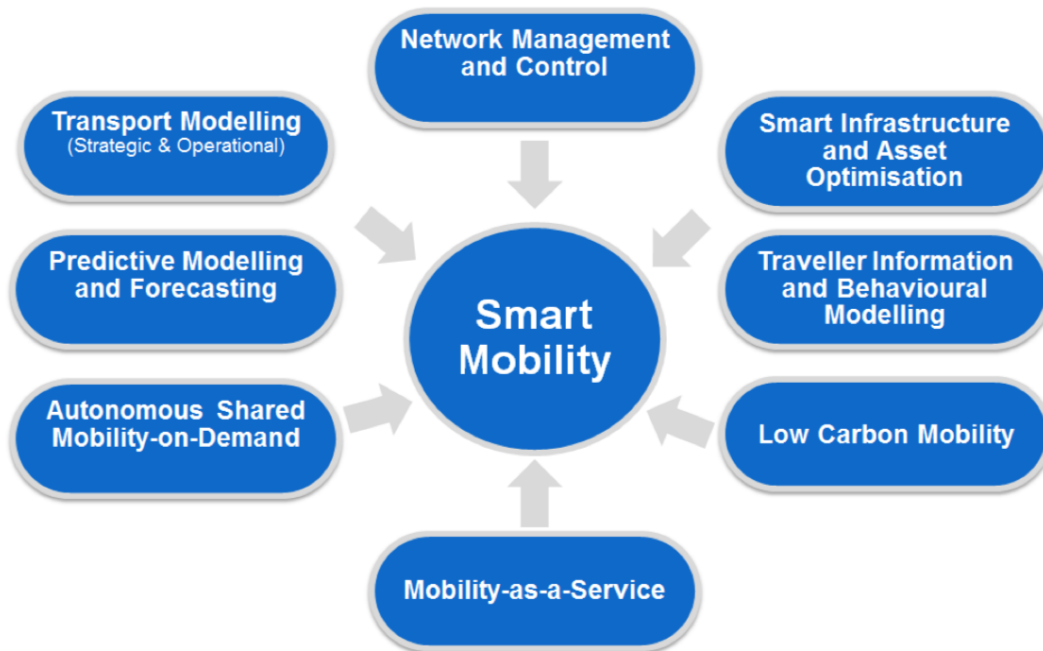


Figure 1: Smart mobility model [3].

Advances in information and communications technology will have far-reaching impacts, making it seamless, and more efficient, eco-friendly and comfortable. Machine-to-machine (M2M) technology will boost the efficiency by using sensors embedded in a wide array of objects and systems to automate tasks and deliver real-time analysis and monitoring. Increases in computer power and the ability to handle the processing of large amounts of data in real time, will lead to more effective use of big data. Big Data and the Internet of Things (IoT) will allow transportation modes to communicate with each other and with the wider environment, it will lead to truly integrated and inter-modal transport solutions [1].

Similar to Smart Mobility, the Smart City concept is a place where traditional networks and services are made more efficient with the use of digital solutions for the benefit of its inhabitants and business. To realize Smart City, wireless sensor networks (WSNs) are required to be widely deployed to monitor our living environments, e.g., the structural health of buildings, the water distributions, or the traffic of urban road as illustrated in Figure 2. As it is known, both data collection and transmission consume energy at the sensor nodes (SNs). Old batteries are required to be replaced by the new ones or to be recharged periodically since the capacity of the battery is limited. Nevertheless, update or recharging of the batteries frequently may not be feasible occasionally. Thus, RF Energy Harvesting (EH) is widely regarded as an appealing solution to bring stable power supply for low-powered wireless devices. Since information and power can be carried by the same RF signals, simultaneous wireless information and power transfer (SWIPT) was proposed for RF EH, which has attracted much attention lately in various wireless communication systems technology [4].

These kind of applications are not limited with RF EH technology. The study [5] presents the concept and approach for establishing a ZigBee stack-based wireless sensor network powered by track-borne energy harvesting system. The rail-side sensors (humidity sensor, accelerometer, infrared detector, and temperature sensor) are connected to the ZigBee end device and powered by the track-borne energy harvester. The data can be transmitted to the ZigBee coordinator and be accessed through webpage on the internet with the help of cloud computing technology.

As the smart city ecosystem broadens, the need to develop current train stations into smart railway systems come into being. The application of the most recent technologies from the communication fields is expected to advance the evolution of such systems through the IoT paradigm. Considering that industrial applications are characterised by strict requirements in terms of reliability and security of railways systems, the adoption of those recent wireless technologies is anticipated to be now mature to implement the IoT technology on a large scale and to restore current wired based communication solutions in the railways sector [6].

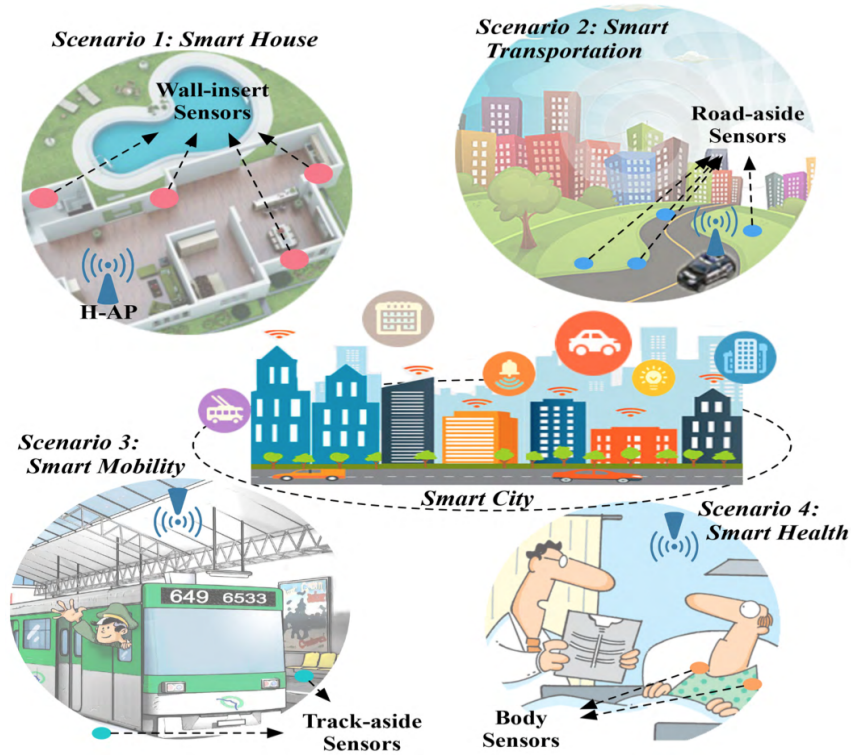


Figure 2: Illustration of smart cities (including smart house, smart transportation, smart mobility and smart health) [4].

Rail traffic systems are extensively acknowledged as an alternative green transportation for goods and people due to their higher energy efficiency, higher mobility and substantially lower environmental impact than conventional transportation systems. In the near future, people will examine further advances in railway systems, such as the development of fully automatic train operation, prewarning for rolling rocks, real-time monitoring and infrastructure, predictive maintenance planning, and highly accurate passenger information. All these are the services in smart rail systems whose aim is not only to improve operation mobility, reliability, and safety, but also to improve quality of service, eco-friendliness, cost efficiency, and comfort [7].

Nowadays, the smart rail implementation seems to be highly interested by industry. For the first time, the World Radiocommunication Conferences (WRC) has published the railway train-to-ground communications in WRC-19. IEEE has also issued a series of standards to support the development of smart rail communications. It shows that the railway industry is now looking into wireless communications with great interest. Both academia and industries have developed many initiatives that focus on communications technology to fulfill the goals for the future smart railways.

The issue of train operation safety has attracted more and more attention with increased train speed. The moving body (e.g., train), the ground infrastructure (e.g., trackside equipment), and the signaling system are in general the three main parts contributing to the high-speed railway operation safety. Of these three parts, the train operation control system, is the key part and is regarded as the nerve center of the high-speed railway system. Maintaining a reliable communication link between the train and the ground, dedicated mobile communications play a key role in order to make the train operation control system work better. With the fast growth of railway services, broadband communication systems for railway called long-term evolution for railway (LTE-R) will be deployed. Except for the train control data transmission, LTE-R is also expected to offer passengers services such as internet access and high-quality voice or mobile video broadcasting [8].

Among many problems in the field of smart transportation and tracking systems, the localization of the charters in the industry is the one that interests this thesis. The industry demands to know which and how many charters are attached to every main carriers that have the main source of energy. Knowing location of all carriers allow them to ensure transportation progress and safety of goods. This problem can be solved by attaching wireless modules to each charters. The modules would send their identification and location to a central station in certain frequency.

Long-distance radio (LoRa) is a kind of extreme distance wireless transmission scheme based on spread spectrum technology. It is part of one of internet communication technology, with low cost, long distance, low power consumption, easy deployment. The transmission distance can reach 1-3 km by improving the receiving sensitivity in the complex city and it can solve the problem of locating base station cable communication wiring inconvenience, which improves the flexibility of base station layout [9]. Although it has range of few kilometers in urban areas, it is also suitable for long range communications since it can reach 15-20 kilometers distances. LoRa is often used in sensor readings, agricultural monitoring, meter reading or smart cities.

Furthermore, since the IoT technologies are emerging, industrial and consumer systems are required to detect and localize tagged items with high accuracy using cheap, energy autonomous, and disposable tags. The paper [10] discusses system-level and circuit-level aspects to be adopted for future generation passive radio-frequency identification (RFID) tags with localization capabilities. In order to achieve this purpose, it is highlighted that RFID-enabled localization strategies, combination with ultra-wideband (UWB) backscattering for localization purposes and UHF for powering of battery-less tags can be profitably utilized.

Especially in the automotive and robotic sectors, the real-time sensing of distributed mechanical parts would be counted as one of the main challenges for the industrial IoT paradigm. For example, rotating and moving operations could be partially attainable so that they are achieved using wired interconnections which makes it quite difficult to be accessed. These limitations are considered to be overcome using an autonomous wireless node that is proposed in the work [11]. It is known that metallic objects can compromise a wireless monitoring system reliability but the presented design of a novel battery-less node which utilizes the LoRa protocol in the 2.4 GHz has been demonstrated to be successfully operated even in this kind of harsh environment.

The study [12] introduces the application of LoRa LPWAN technology in sailing monitoring system to track the environment of sea and sailboat, including the speed and direction of wind and current, the location and attitude of sailboat. It is required to cover the distance between the sink nodes and the base station which corresponds to at least two kilometers. Besides, the system faces the challenge of insufficient power supplement at the sea. This means that it would rely on the batteries for a long period of time, therefore the system should maintain low power consumption.

One of the important fields of IoT utilization is in transportation known as intelligent transport systems. Smart transport applications can manage traffic in cities and between the cities and can reduce traffic congestions, optimize parking, reduce accidents. The paper [13] proposed a model that is the roaming mechanism developed for international shipment tracking and cooperation between multiple shipping companies. This mechanism manages roaming when the vehicle of a shipping company from country A connects to a LoRaWAN network of a shipping company from country B. The classical LoRaWAN network used by only one operator is shown in Figure 3.

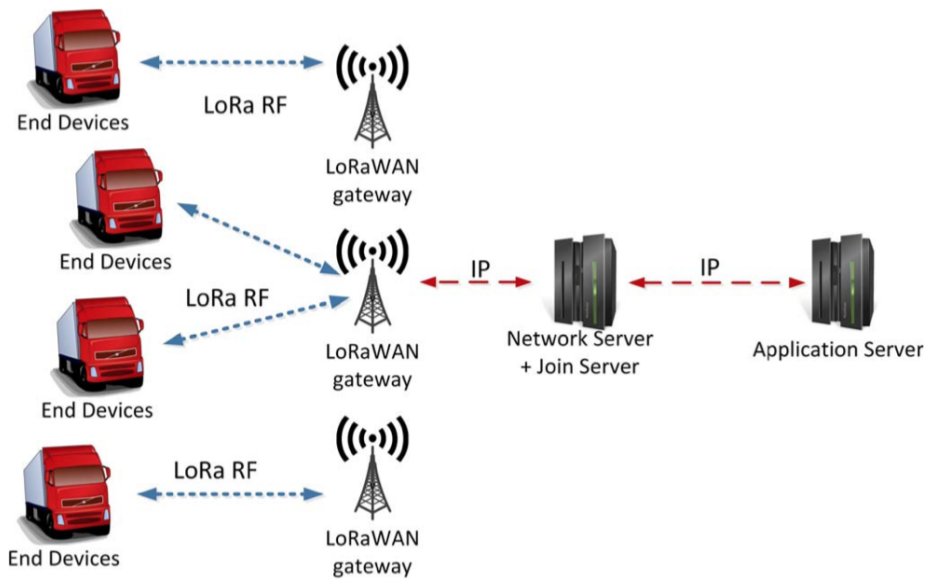


Figure 3: Typical LoRaWAN network of a shipping operator [13].

Moreover, seaports act as the essential business player for supporting the global supply chain system and enormous number of activities may occur daily within this large area, primarily the loading and unloading processes. Therefore, time is an integral parameter in a seaport, where a truck must be available right before the ship arrives. Applying IoT technologies reveals a potential solution to solve this challenging industrial use-case. Figure 4 illustrates the suggested solution, which shows the usage of the localization system. The approach aims to achieve efficient and precise decisions for yard management and vehicle dispatching. The trucks in Figure 4 are coordinated by the terminal operating system, that uses the information received from the LoRa gateway. While moving to the appropriate container block destination, the information is sent by each truck. The proposed system allows the port authorities to minimize traffic congestion, heighten the safety of all entities, and improve the yard management in the seaport area [14].

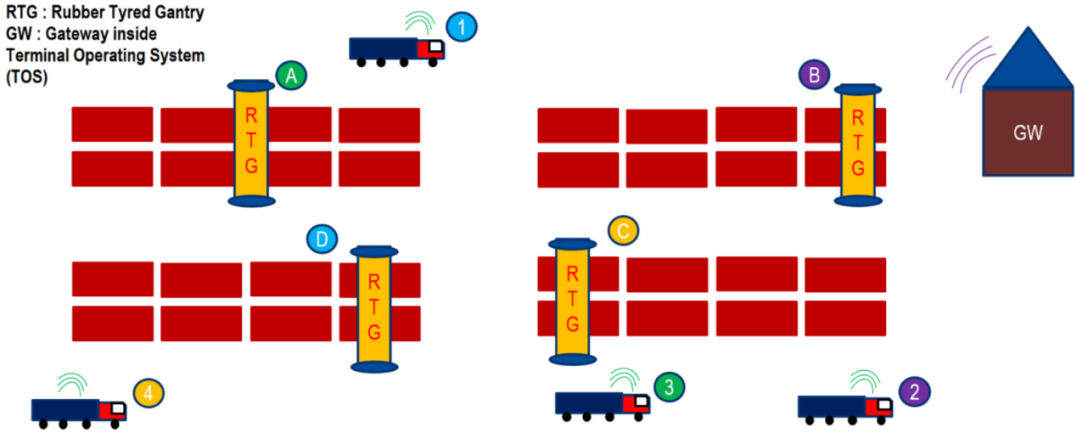


Figure 4: Harbor use-case: truck and asset localization [14].

As the IoT drives the emergence of many new smart “things” that need to be recharged, and with the prospect of smaller batteries for sustainability, wireless charging could help to overcome some of the challenges involved with recharging small devices. Also, product designers are able to eliminate any need to provide a port such as a micro USB socket or 2.5 mm coaxial jack in the side of the enclosure for connecting the charging cord. This brings several advantages, including simplifying the design of the enclosure and saving bill of materials costs by eliminating the mechanical mountings for the charging socket. An aperture-free enclosure can also be sealed more easily thereby helping to simplify splash-resistance or water-proofing. In some applications, such as industrial process-monitoring equipment, charging could even be automated using a simple mechanism to bring a power transmitter and battery-powered smart sensors close together at regular charging intervals [15].

Any type of industrial plants may require such an above-mentioned localization system and in particular, this thesis suggests a battery-less solution to solve this challenging problem in railway industry. Using wireless power transfer (WPT), we eliminate the problems that arise by having batteries such as charging or having high-capacity batteries. This feature also adds the system interchangeability so that the wagons can be changed conveniently. The mechanism requires LoRa modules to each trailers as illustrated in Figure 5. Starting with the main trailer which has the main source of energy, the power will be transferred via a transmit antenna at the back of the carriers and will be collected via a receiving antenna at the front. Power divider on each receiver will portion certain amount into LoRa node and the rest will be carried onto next transmitting antenna by cables.

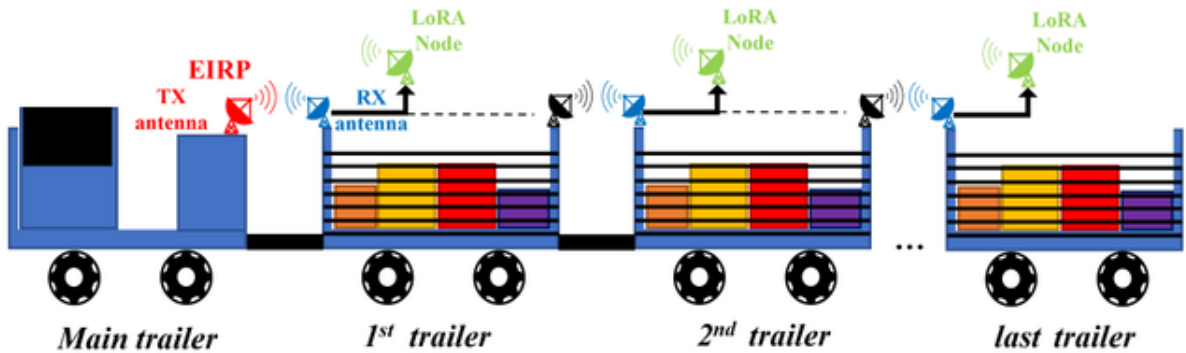


Figure 5: Visualization of the overall system.

Since the LoRa nodes need DC power, every receiving antenna has rectifier circuit which creates a rectenna (rectifying antenna). A simple rectenna element consists of a dipole antenna with an RF diode connected across the dipole elements. The diode rectifies the AC induced in the antenna by the microwaves, to produce DC power, which powers a load connected across the diode. Schottky diodes are usually used because they have the lowest voltage drop and highest speed and therefore have the lowest power losses due to conduction and switching [16]. Large rectennas consist of arrays of many power receiving elements such as patch antennas. For this project, it is also intended to design an array embedded with a high number of antennas in order to increase the antenna gain. In addition, the rectifier must be quite efficient. However, designing a powerful rectifier would be harder than expected because the power received at each antenna will be intentionally different. As we pass more and more carriers, the amount of power decreases. Since rectifiers are non-linear circuits, their behavior is related to the input power. Therefore, the design must be done very carefully and detailed.

For the antenna design, two distinct types of array are proposed: array of monopoles and patch array. They are discussed in details within designated chapters where focus has been given to the overall antenna dimensions, which need to be compliant with the environment in which they are located, in this case the back and the front of the charters. Furthermore, working mechanism of LoRa modules are required to be studied in order to decide on power splitter layout. The power needed to send basic identification and location must be known and then power division ratio has to be determined. Commercially available power splitter component could have been used but it has been decided to design a coupled line for the splitting since it is more controllable and less costly.

The main goal of all these design criteria is to supply power as many LoRa nodes as possible. Thus, a separate chapter and attention has been given to power budget evaluation. The most promising designs have been assessed in order to compare the number of LoRa modules that can be charged in acceptable time. Of course, this charging time is degree of freedom that we can change and it depends on how frequent the communication is desired.

2 LoRa Module

LoRa is a communication technology widely used in the current low-power wide area network technology. It mainly includes two bottom layer structures: physical layer and MAC layer as shown in Figure 6. Its characteristics consist of low power consumption, large channel capacity, anti multipath fading and anti Doppler effect. The LoRa carrier frequency is the lower ISM band (137-1020 MHz), which operates in the global free frequency band, including 170 MHz, 433 MHz, 868 MHz, 915 MHz, 915 MHz, etc. [17].

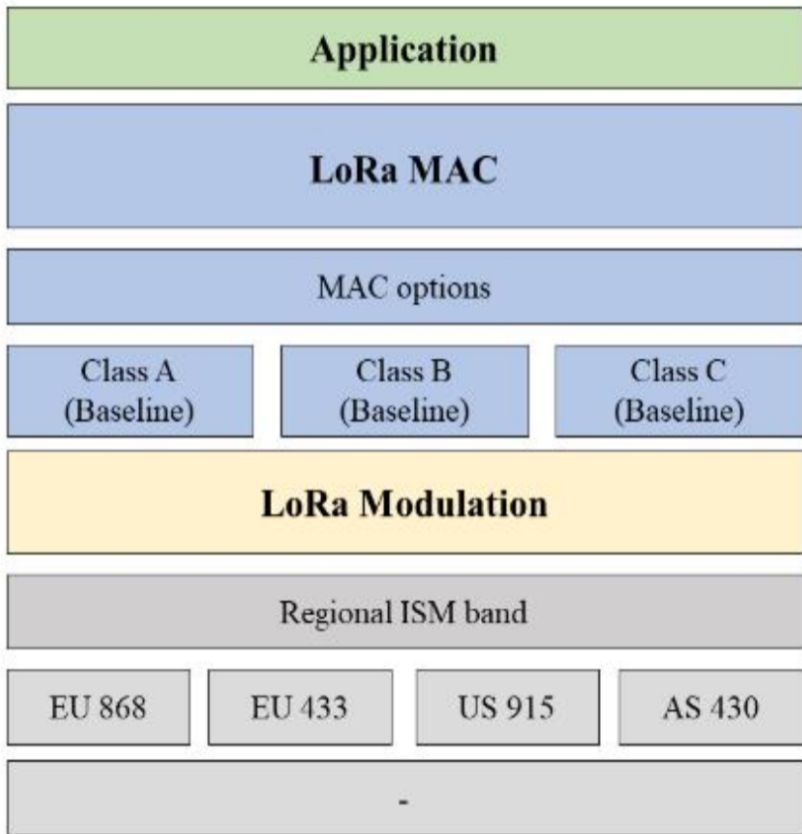


Figure 6: LoRa hierarchy [17].

LoRa and LoRaWaN are sometimes used in the same sense but this is actually a misunderstanding. LoRa presents the physical layer for the long distance connections, while LoRaWaN is defined as the connection protocol and the system architecture. Figure 7 shows the architecture of LoRaWan. As a trademark registered by Semtech, LoRa transfers data from one point to another for the Low Power Wide Area Network (LP-WAN) using the chirp spread spectrum (CSS) and by doing that LoRa can significantly increase communication range while maintaining robustness to interference. It should also be noted that LoRa shows better immunity to interference due to sub-GHz radio spectrum [18].

One of the ability of LoRa is to change the spreading factor (SF) during communication. The best spreading factor is selected according to the environment or the distance between the gateway and the device with the help of adaptive data rate (ADR) [19]. Therefore, the data rate changes between 0.3 Kbps and 50 Kbps. By doing that, the system can be used in the most efficient way by extending the battery life.

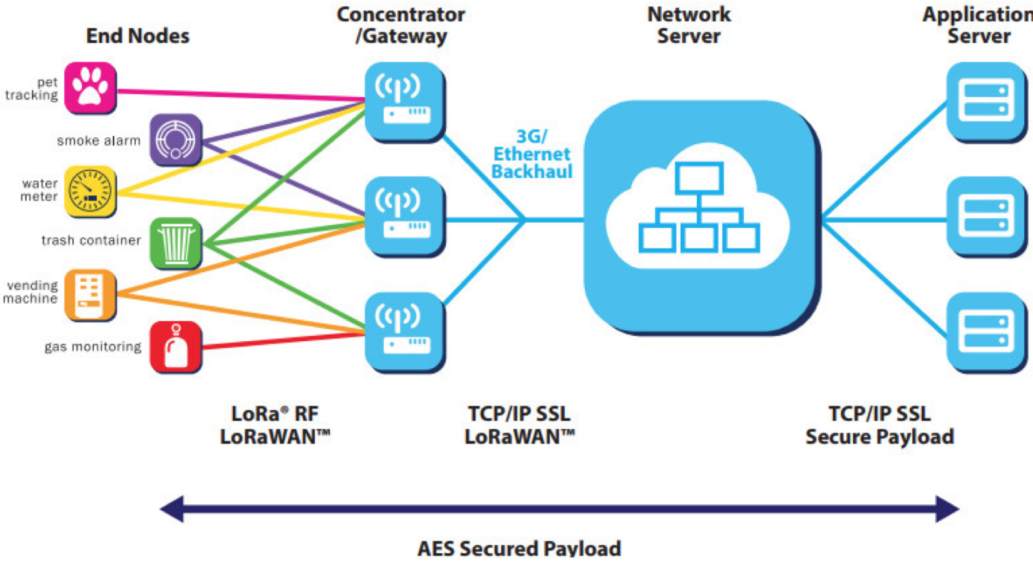


Figure 7: LoRaWan architecture [20].

LoRa uses two types of packet formats which are called explicit and implicit. The explicit packet includes a short header that contains information about the number of bytes, coding rate and whether a Cyclic Redundancy Check (CRC), used for error protection, is used in the packet. The LoRa packet encompasses three parts; a preamble, optional header and data payload, as shown in Figure 8. Additionally, Forward Error Correction (FEC) schemes can be activated. These characteristics are attractive for many IoT applications, and many regions and countries are trying to accept the LoRa technology on their regional ISM band.

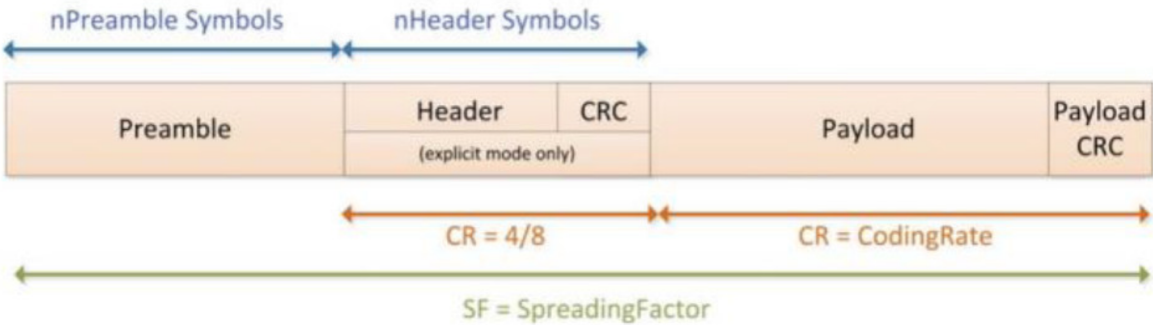


Figure 8: LoRa packet format [21].

The above-mentioned technologies are actually well known from the last decades in mobile communication, however they are now used for the first time in cost-efficient and low power short range wireless networking. The spread spectrum modulation, in contrast to the legacy modulation techniques, leads to an increased link budget and better immunity to interference. For this purpose, LoRa utilizes broad-band linear frequency modulated pulses to achieve good frequency characteristics [22].

Although short range wireless communication explicitly targets local and very regional applications, range continues to be an extremely important issue. The range directly depends on the so called link budget, which can be increased by the choice of modulation and coding schemes. The study [22] also shows free space measurements with LoRa technology. It presents measurement results with different test cases and with various payload lengths. For the sake of payload length, we may refer to the lowest amount in this project since the information we need from every carrier is the simplest possible.

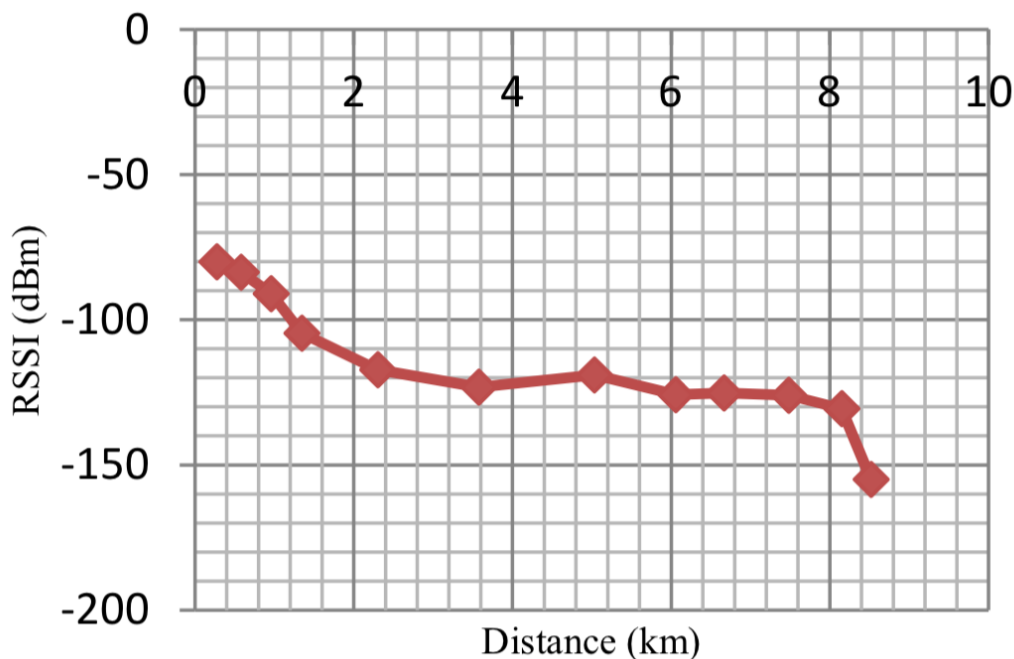


Figure 9: RSSI measurement values with payload length 10 bytes [22].

Figure 9 shows some received signal strength indicator (RSSI) measurements with payload length 10 bytes in typical case using spreading factor 10, bandwidth 250 KHz, coding rate 4/6 which leads to bit rate of 1627.6 bps. The results are quite similar in the case of a payload length 50 and 100 bytes. One can observe from the plot that -120 dBm is maintained almost constant for a wide range of distance and there is a significant drop of RSSI after 8km. These confirm that long distance range has been kept with proper receiver sensitivity. Although we mentioned the range aspect of LoRa, this thesis

pays more attention into the perspective of the module power consumption. Since this project plans to transfer power from the carrier with the main energy source to all, the last carrier has to be guaranteed to power its LoRa device. The energy budget evaluation will be discussed in later chapters but power need of a LoRa module must be known for a basic identification transmit.

One of the most important features of LoRa is its low-power communication capability. Having low-power capability is very attractive for a variety of IoT applications. As shown in Figure 10, to measure the power consumption, each cycle can be divided into three states (TX state, RX state, SLEEP state) and the consumption current can be integrated according to each state into each state time. The power consumption was calculated by multiplying the power consumption by the power consumed during one hour [23].

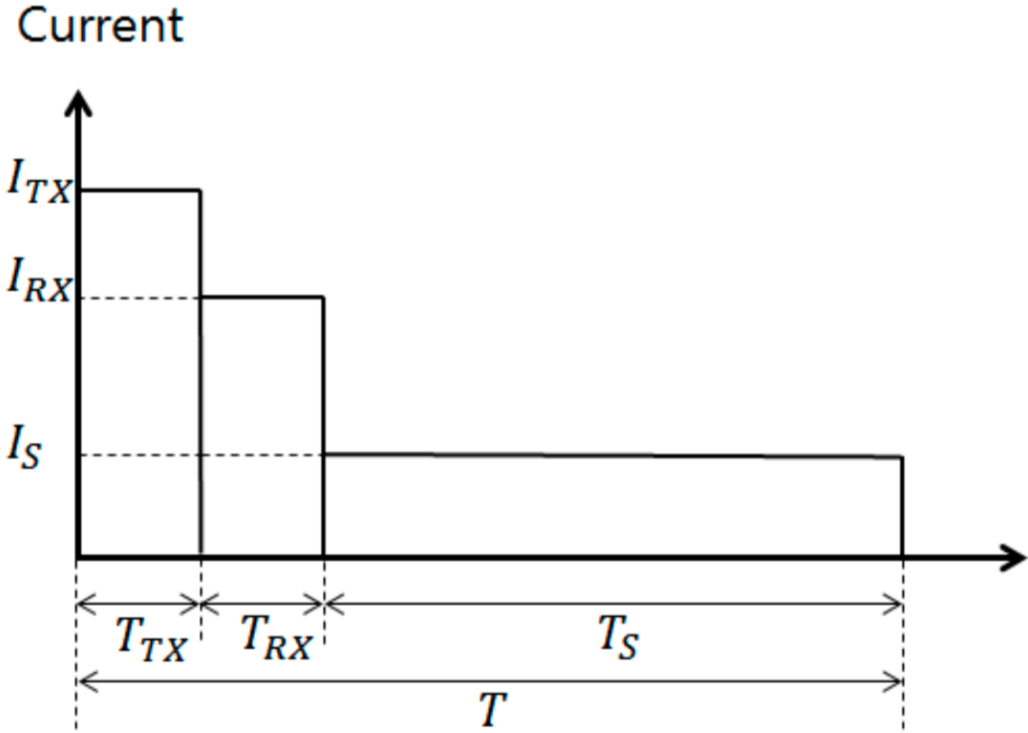


Figure 10: Power state in terms of communications [23].

Figure 11 shows the results of increasing the number of data transfers per node from 1 to 10 for one cycle (1h). Note that cooperative downlink listening (CDL) is an extended version of the standard LoRa, yet it accommodates all of the low-power features in LoRa, so the energy consumption of each node is not significantly different. One can understand from below figure that energy consumption of 0.05–0.44 mJ are obtained for a device running when transferring data from 1 to 10 times per hour.

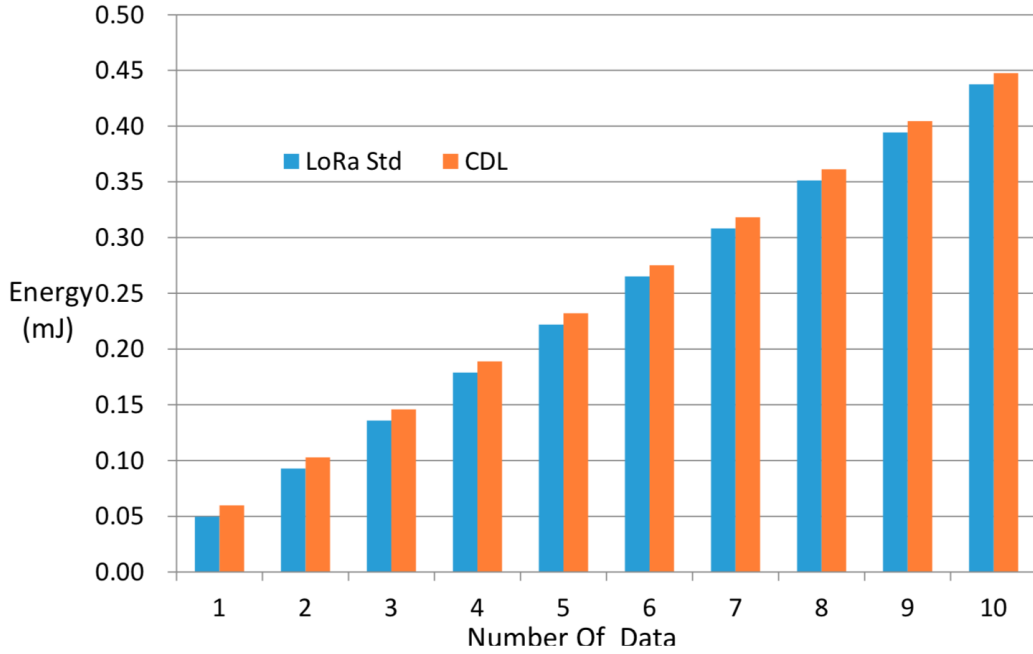


Figure 11: Energy consumption of LoRa [23].

Furthermore, the result of study [12], that is mentioned on the introduction section, about coverage shows that greater bandwidth or the smaller SF can increase the range at the expense of an increase of delay and decrease of data rate. For instance, bandwidth of 125 kHz and SF of 7 and are used in sailing monitoring system to meet the trade-off of data rate, link budget and coverage. At one particular case, it shows that LoRa technology in the system has a good performance in mobility with 20 km/h average speed. At the same time, LoRa technology is affected by obstacles such as trees or high buildings, which lead to the high packet loss rate of over 20% in those zones. For that reason, these factors should be taken into consideration when LPWAN LoRa network are implemented. When the environment changes, either better or worse, the parameters of LoRa technology such as SF and BW can be changed automatically to improve the sensitivity, interference immunity and coverage.

3 Antenna Design

After defining the reasons behind the choice of a LoRa node for this type of applications, this chapter aims to describe the design of the antenna step in details. There are many types of transmitter antenna each of which has its own benefits. Some examples are: the slotted waveguide, microstrip patch and parabolic dish antennas, which are able to have high directivity and efficiency. By using not only high directivity but also high gain antennas within a WPT systems, the propagation loss can be compensated and the power could easily be transferred to any place, making the system more efficient. With the rapid development of wireless communication technologies, highly advanced antennas have been investigated, which include low-profile, light weight and reconfigurable characteristics [24].

Microstrip antennas have several advantages, including reduced size and weight. Since they can be manufactured using printed circuit technology, their can have low production costs. These types of antennas provide a good versatility in terms of polarization, impedance and resonance frequency. On the other hand, microstrip antennas have disadvantages such as low efficiency and low power; however, these disadvantages can be overcome by using antenna arrays.

An antenna array is a set of two or more antennas. The signals from the antennas are combined or processed in order to achieve improved as compared to single antennas. The antenna array can be used to increase the overall gain, provide diversity reception, cancel out interference from a particular set of directions or steer the array so that it is most sensitive in a particular direction. In general, the performance of an antenna array increases with the number of antennas, or elements, in the array; the drawback of course is the increased cost, size, complexity and radiation efficiency.

As it described in the introduction section, the distance at which the power will be transfer is approximately one meter. The gap between consecutive carriers might be less than this but taking into account one meter would ensure the performance for any scenario. Since it is desired to power as much carrier as possible, achieving high gain is one of the main objectives that need to be addressed during the design of the TX and RX antennas, explaining why the array topology has been chosen.

The first problem with the antenna design has been the choice of the operating frequency among the possible ones: 868 MHz, 2.45 GHz and 5.8 GHz. As it is known, they are ISM radio bands and give us flexibility for regulation issues although it may create interference problems. These frequencies must be evaluated considering how the corresponding free space attenuation can reduce the received power when a certain distance is considered. This can be preliminary and easily done by using the Friss formula:

$$P_r(d) = P_t \frac{G_t G_r \lambda^2}{(4\pi d)^2 A} \quad (1)$$

where, P_r is the received signal power in Watts expressed as a function of separation distance (d meters) between the transmitting and the receiving, P_t is the power of the transmitted signal's Watts, G_t and G_r are the gains of transmitter and receiver antennas when compared to an isotropic radiator with unit gain, λ is the wavelength of the carrier in meters and A represents other losses that is not associated with the propagation loss.

One can easily see that low frequency means low loss in free space, however it would lead to a larger antenna as well and this creates a problem for limited area cases as we have. The antenna array must fit into certain dimensions since it is designed to be placed on the back and the front of the wagons. Furthermore, the bigger the antenna array, the more the cost since there has to be used more materials, especially the dielectric substrate.

The first frequency that is discarded among all is 5.8 GHz since it would give considerably high path loss comparing to the others. Also, some simulation results from a previous work with similar objective show that 5.8 GHz would not be suitable a choice of this project. Also, exploiting monopole antenna arrays has been considered especially for their design simplicity. Full-wave simulations to design and characterize the various antenna layouts have been carried out. By using the 3D electromagnetic (EM) software, the performance of the arrays have been analyzed also in the case of varying the type of substrate, its thickness and the number of elements within each array.

| 2.45 GHz SOLUTIONS | | 868 MHz SOLUTIONS | |
|---|--|--|--|
| PROS | CONS | PROS | CONS |
| Reduced dimensions 46x48x0.15 cm³ | Higher path loss 40.22 dB | Lower path loss 31.21 dB | Large dimensions 46x48x8.6 cm³ |
| | Higher cable loss Best case 3.36 dB/20m | Lower cable loss Best case 1.9 dB/20m | |

Figure 12: Frequency comparison.

Figure 12 compares the two designs at the two operating frequencies: 2.45 GHz and 868 MHz, underlining both advantages and disadvantages. Another important aspect that is highlighted from Figure 12 is the coaxial cable loss. A chapter is dedicated to the cable selection later in this paper but it can be preliminary seen that, working at higher frequencies would imply having higher cable loss and this is an important parameter to be accounted for when designing a system that is applied in a long-distance range.

3.1 Monopole Array

A monopole antenna has a straight rod-shaped conductor mounted perpendicularly over conductive surface which acts as ground plane. The presence of the ground plane allows the monopole antenna to operate as electrically equivalent to a dipole antenna. The ground plane equivalently replaces the lower half by an imaging principle, similar to creating an optical image through a mirror. The radiation pattern of monopole antennas above a ground plane are also known from the dipole result. The only change that needs to be noted is that the impedance of a monopole antenna is one half of that of a full dipole antenna.

First, a single monopole is designed for 2.45 GHz as shown in Figure 13. It has straight feeding line and a correct tuning allows to have good performance for radiation efficiency and gain. A background plane is also placed in the back indicated with yellow color and it helps to reflect the power that would go toward opposite direction. This increased the performance significantly. The dielectric substrate that used for this preliminary analysis is FR-4, which is a cheap and basic substrate material.

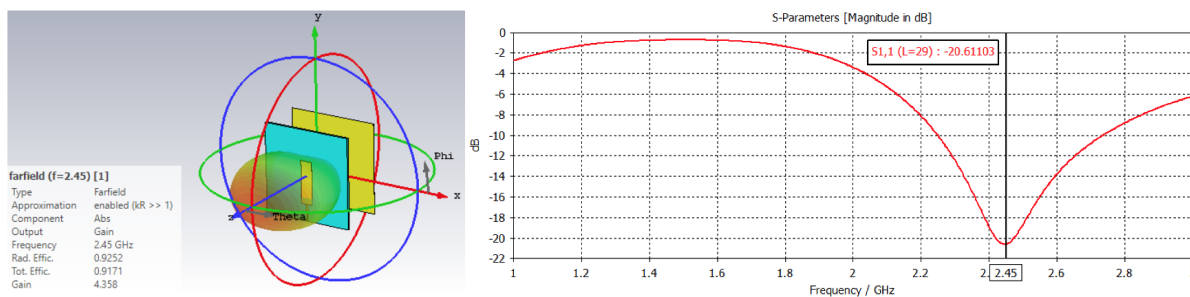


Figure 13: Single monopole.

Moreover, 2x2 antenna design has been simulated and shown in Figure 14. With more than one element, the feeding structure becomes more complicated and requires specific expedients to guarantee a correct functioning. Note that 180° phase shifter has been placed on the lower branch of the feeding line. This would result in constructive radiation pattern in $z(+)$ direction. Also, secondary lobes are present slightly around 3 dB less than the main one.

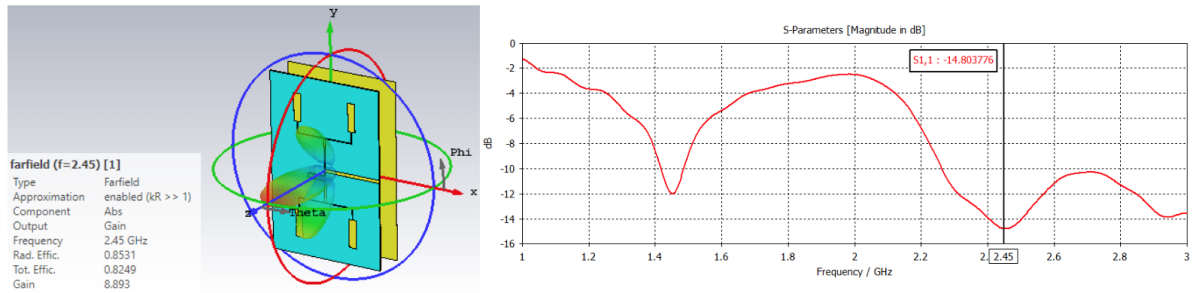


Figure 14: 2x2 monopole.

Subsequently, the vertical distance between the upper and lower branch has been shorted as close as possible to $\frac{\lambda}{2}$ in order to reduce the secondary lobes. After reducing the vertical space by meandering the monopole feeding lines the radiation diagram changes with a consequent degradation both on the input reflection coefficient, which shows a drastic detuning, and also on the radiation diagram, as depicted in Figure 15.

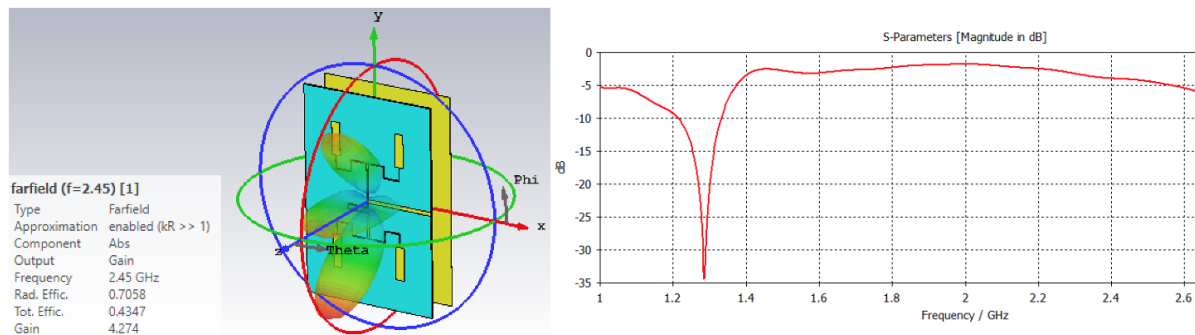


Figure 15: 2x2 monopole with meandered feeding.

In order to separate the horizontal part of the feeding line from the back copper ground, some analysis have been made to observe the effect of increasing the feeding line of the single monopole together with the back copper plane. The results highlight a shift in the resonance frequency. Therefore one can conclude from it that the length of the feeding line of the monopole has influence on its resonance frequency.

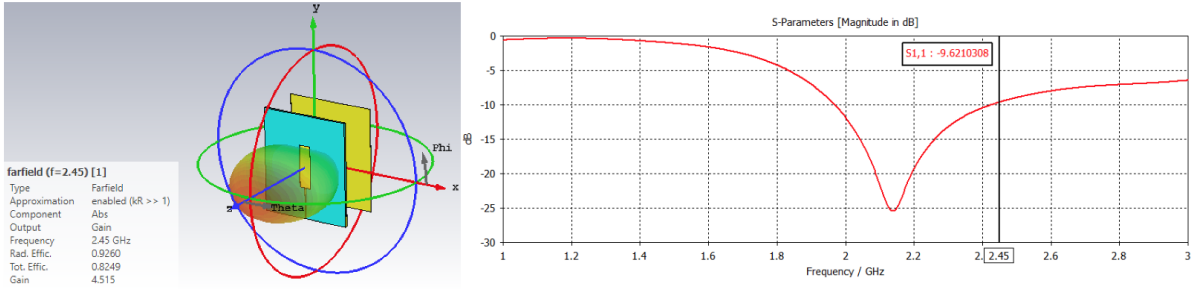


Figure 16: Single monopole with longer feeding.

Then, the same length feeding line is meandered and simulated. The results in Figure 17 show another shift in the resonance frequency of the monopole.

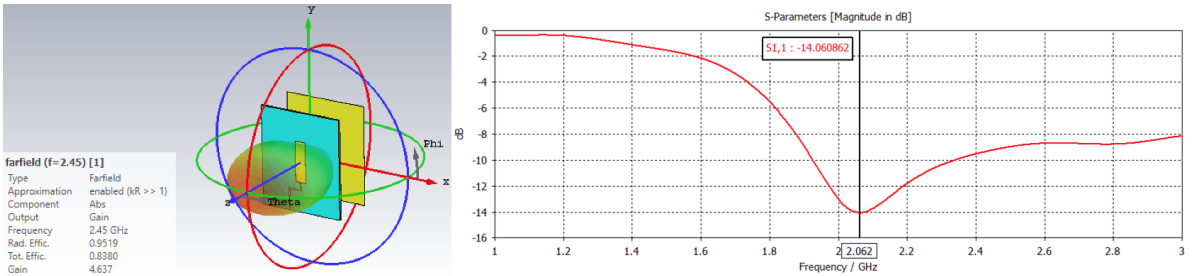


Figure 17: Single monopole with longer meandered feeding.

Furthermore, the 2x2 monopole with meandered feeding line is created and the ground plane is extended in order to contain the horizontal line. Figure 18 illustrates that the radiation pattern varies, and the resonance frequency is shifted considerably.

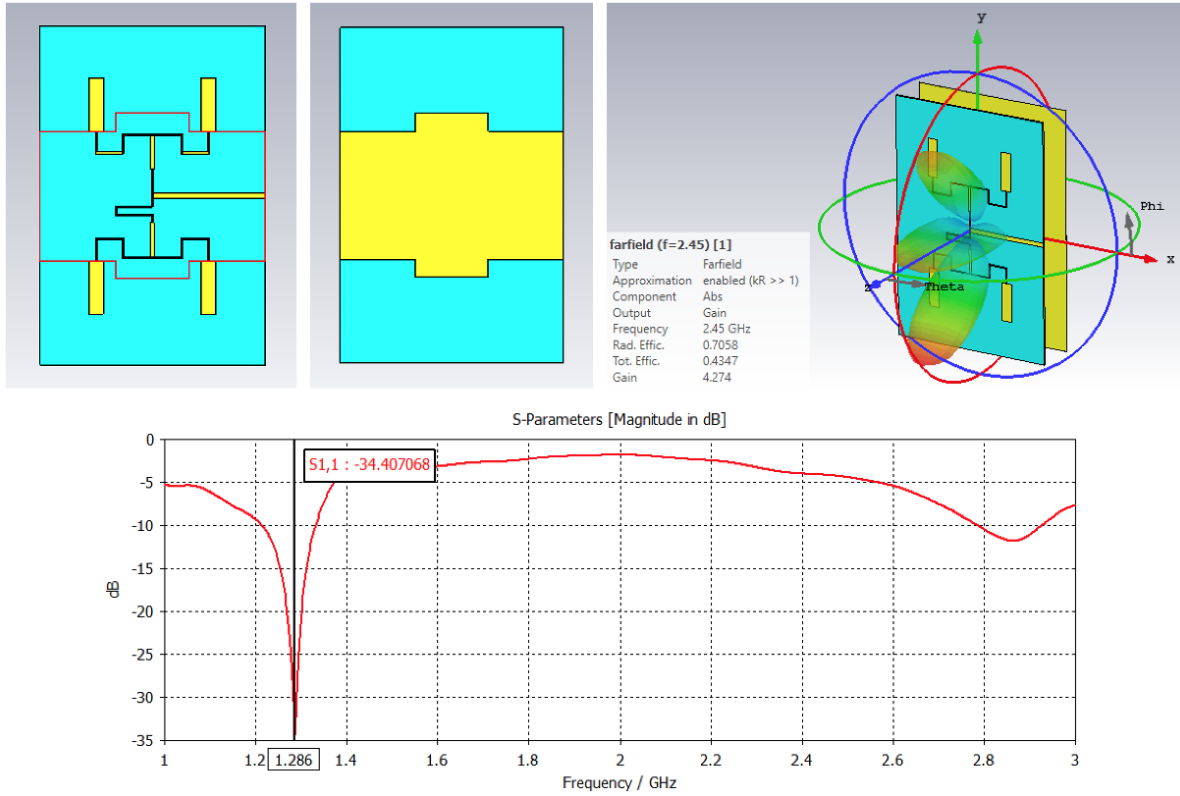


Figure 18: 2x2 monopole meandered with extended ground.

The straight feeding line configuration has been then selected for the 2x2 monopole array, whose performance are reported below and the shift in resonance frequency can be easily solved by by acting on the monopole length for retuning the array.

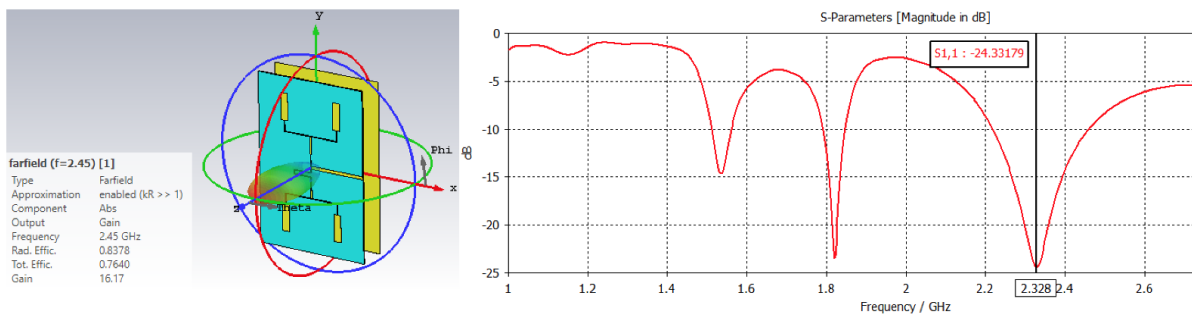


Figure 19: 2x2 monopole with straight feeding line configuration.

As the antenna gain is quite good, 4.27 dBi, for the 2x2 monopole configuration we opted for the design of a 8-monopole configuration and the re-tuning has been made by reducing dimension of the monopoles. However the reflection coefficient and the antenna input port (S11) has not shown improved results as illustrated in Figure 20.

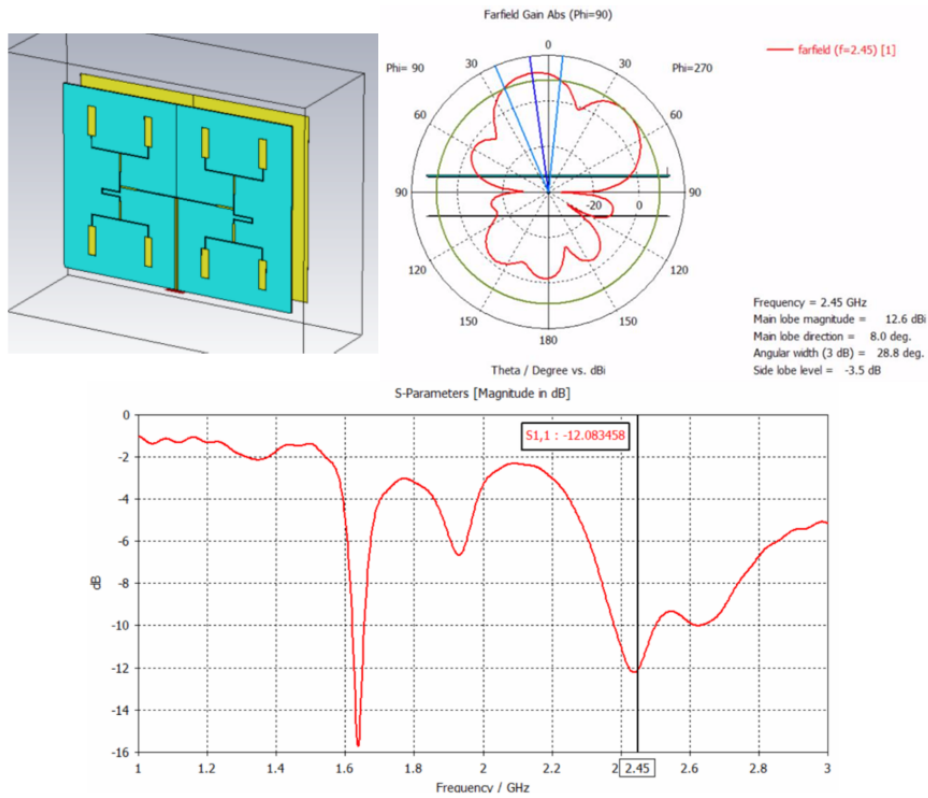


Figure 20: 8-monopole results.

By keeping the design symmetric, the number of elements has been increased to 16. The results have been promising for further developments as it can be seen in Figure 21 where a gain of 15.8 dBi and a radiation efficiency of about 71% are highlighted.

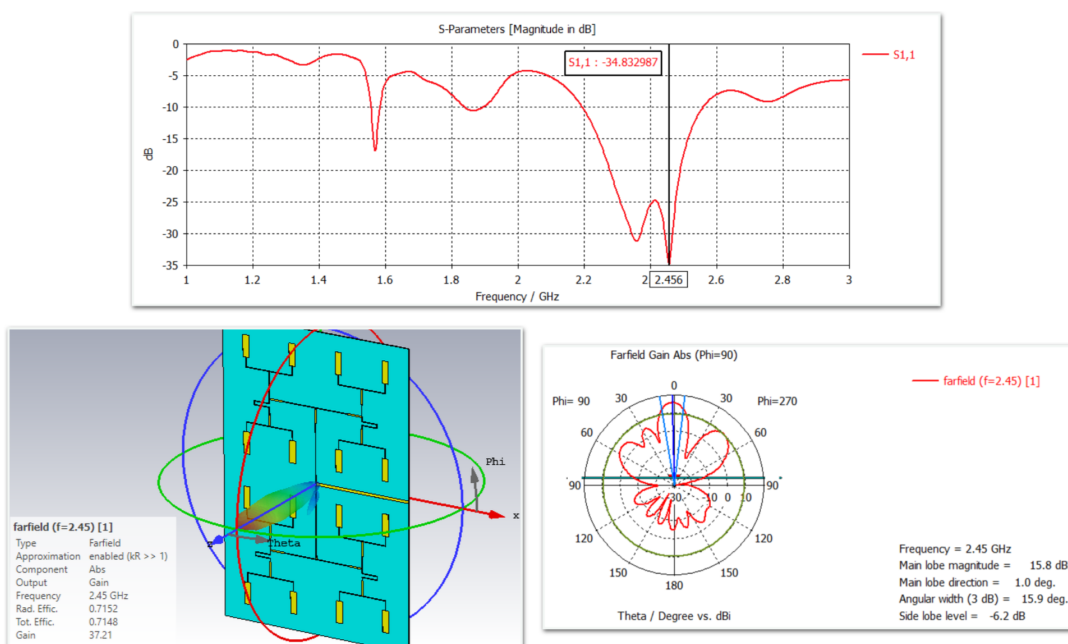


Figure 21: 16-monopole results.

Before going into further enhancements, another design with 868 MHz has been constructed as illustrated in Figure 22. Although the radiation outcome was acceptable for 16 elements, the size was much larger than 2.45 GHz one. Since the dimensions we would obtain for higher gain would be quite large, 2.45 GHz has been selected as a more suitable operating frequency.

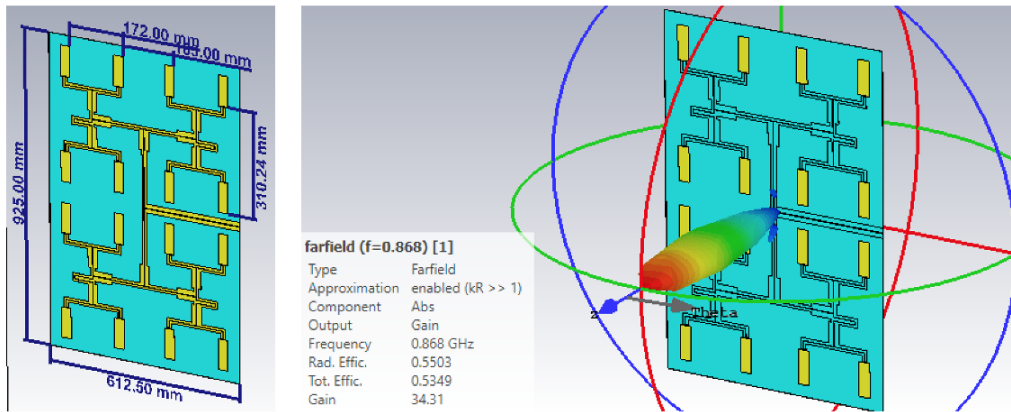


Figure 22: 16-monopole results.

The ultimate design using monopole antennas has shown in Figure 23. We have obtained 61% of radiation efficiency and approximately 18 dBi of antenna gain. Despite the fact that the dielectric substrate is FR-4, we have constructed relatively powerful monopole antenna.

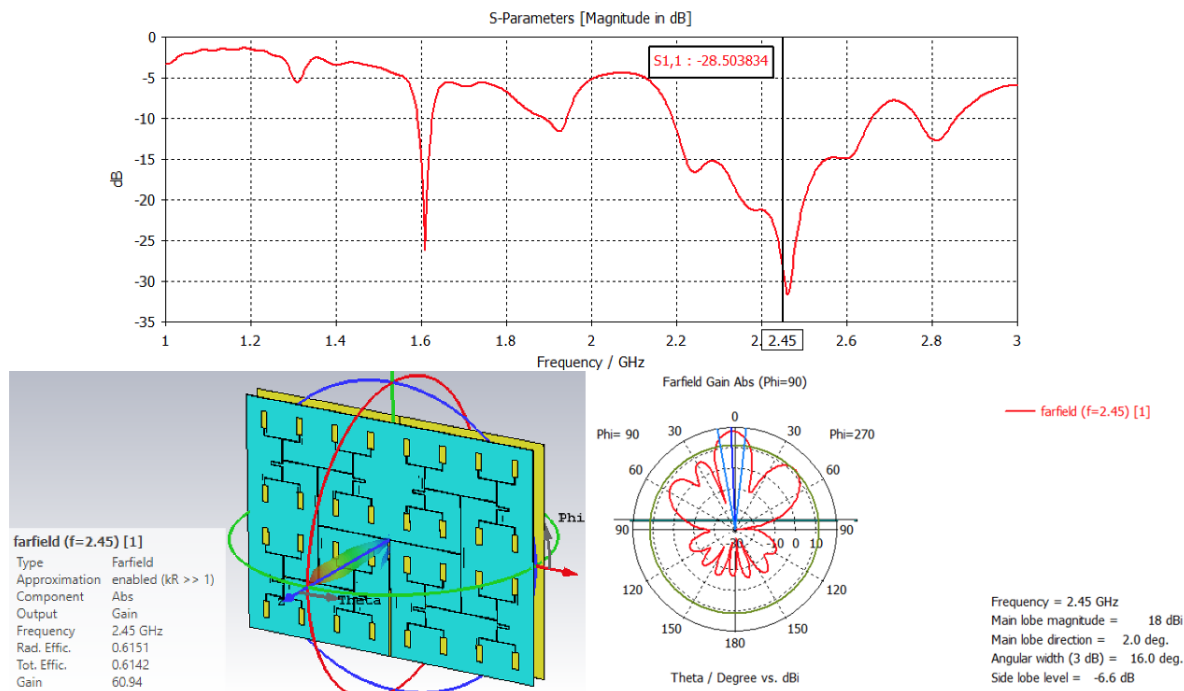


Figure 23: 32-monopole results.

Figure 24a illustrates some important dimensions of the design and indicates which lines correspond to which impedance value. In Figure 24b, a unique structure of the ground has been shown. This specific shape for the ground plane has been chosen in order to minimize the ground as much as possible so that the power that goes toward back could be reflected by the background plane without interruption. Some dimensions are given in Table 1.

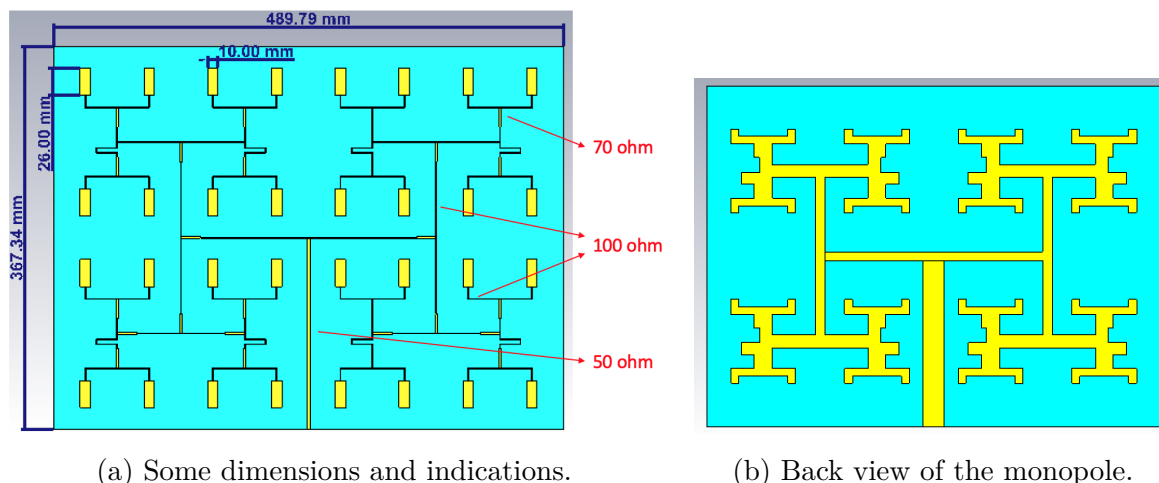


Figure 24: Specifications of final monopole design.

| Name | Value (mm) |
|----------------------------|------------|
| Substrate width | 489.79 |
| Substrate length | 367.34 |
| Substrate thickness | 1.5 |
| Monopole thickness | 0.035 |
| Width of 50 Ω line | 3.3 |
| Width of 70 Ω line | 1.76 |
| Width of 100 Ω line | 0.76 |

Table 1: Parameter list.

After carrying out a thorough analysis of the monopole array performance, we have concluded that the presence of a background plane would force the overall structure to be more bulky and sensitive to the mutual distance between the metal of the train and the monopole. For these reasons, we decided to investigate the performance in the case of a different layout: a patch antenna array.

3.2 Patch Array

The microstrip patch antenna is used in a wide range of applications since it is easy to design and fabricate. In various mobile communication systems the microstrip patch antennas are receiving benefits due to their advantages in terms of low electromagnetic coupling to the human head, low profile, light weight, increased mechanical reliability and high efficiency. The size of a microstrip antenna is inversely proportional to its frequency. The length of the patch is calculated using following formula where λ_0 is the wavelength in free space and ϵ_r is relative dielectric constant:

$$L = \frac{\lambda_0}{2\sqrt{\epsilon_r}} \quad (2)$$

The bandwidth can be improved using a thicker substrate that will increase the surface waves that move through the substrate and radiate the patch. It is known that the antenna impedance will be higher than an accepted value if fed from the edge, and lower if fed from the center. Therefore, an optimum feed point exists between the center and the edge. Most of the models use an inset feeding strategy which does not need any additional matching parts to find this optimal point and this method is considered for this design type.

Single patch antennas can reach directivity values of 7-8 dBi and always have similar radiation patterns. The combination of patch antennas in arrays is frequent and the most popular solution is corporate feed arrays because it is easier to control the feed of each element. In the case of corporate feed network, the power is equally split at each junction of the microstrip patch array antenna for uniform distribution.

Similarly to the approach used for the monopole array, a single patch antenna is firstly designed but this time, we only focus on the 2.45 GHz frequency because of the size limitation again. The expected overall dimensions of the patch antenna at 868 MHz would overcome the ones obtained with a monopole at the same frequency, thus this layout has not been considered.

To obtain high gain objective, parametric analysis of the antennas are performed to identify the best substrate as shown in Figure 25a. Selecting the right dielectric substrate is a trade-off: on one hand, we need to have high gain and high efficiency, on the other hand, it should not be expensive to construct a prototype. For convenience, we have first considered the substrates that we have already owned in the laboratory: FR-4 and Rogers RO3003.

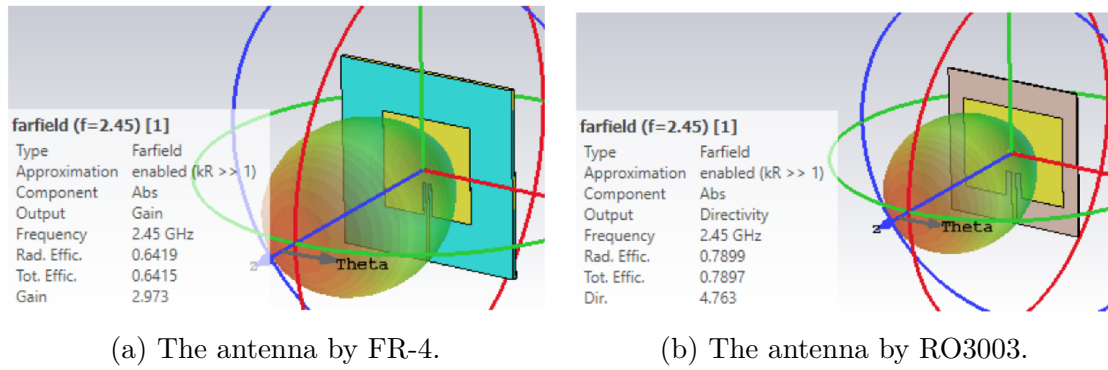


Figure 25: Single patch antenna with different substrates

The radiation result in Figure 25a is by FR-4 material whose characteristics make it very versatile at an affordable cost; in Figure 25b, the result is by Rogers RO3003 which is ceramic-filled PTFE composites and rather expensive. Subsequently, the ITERA MT-40 has been investigated as a suitable alternative to the previously-mentioned substrate, both for the good dielectric properties and for its cost-efficiency. For these reasons, The ITERA MT-40 has been the chosen substrate on which all the following design and analysis have been based.

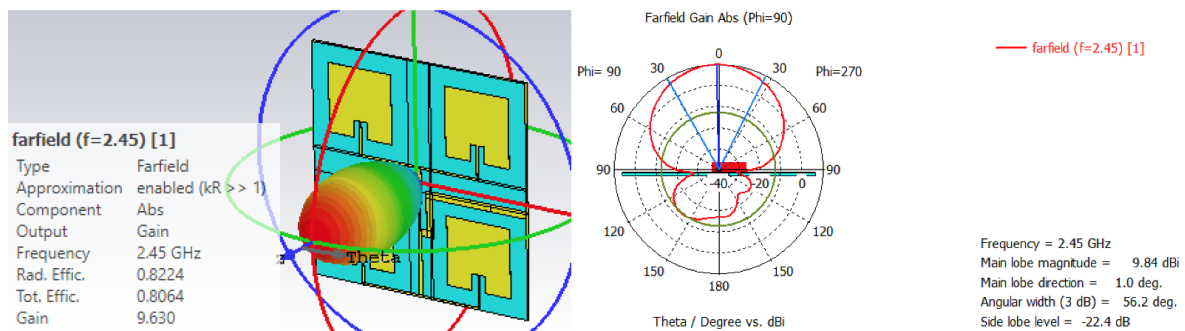


Figure 26: 2x2 patch antenna by MT40.

The single patch full-wave simulation has been made and the result of 2x2 patch antenna design has been shown in Figure 26 above. The size and complexity requirements allow us to have maximum of 64 patches in an array. Above this value is both quite large and also difficult to manage. Having a higher array would lead to extremely large dimensions that can imply difficulties in the overall management of the system. The design with 64 patches is illustrated in Figure 27 below. The radiation efficiency and gain parameters are quite satisfying. For planar array, when the inter element spacing is equal or greater than half of the wavelength, multiple side lobes other than the main lobe will be formed. This rule has been followed so far but the spacing in the middle, the distance that separates the left 32 patches from right ones, had to be shortened to

fit the whole design into the substrate whose dimensions are fixed in the market. Note that we have also designed and evaluated a 16-patch one but it is omitted for the report.

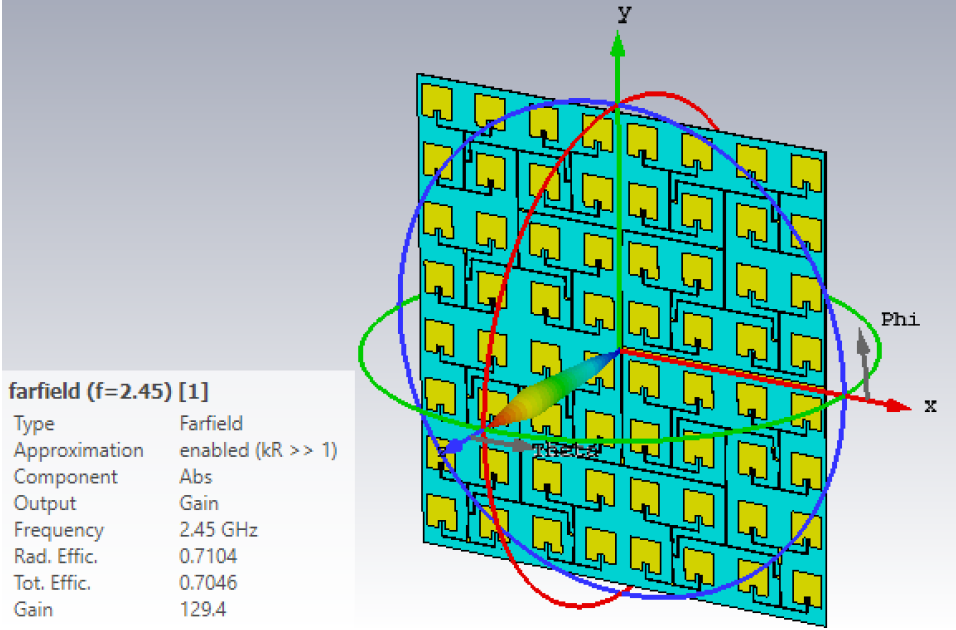


Figure 27: 64 patch antenna by MT40.

The achieved antenna input reflection coefficient (S11) shows good performance, as shown in Figure 28, and no other significant resonances are present in the simulated 1-4 GHz frequency range.

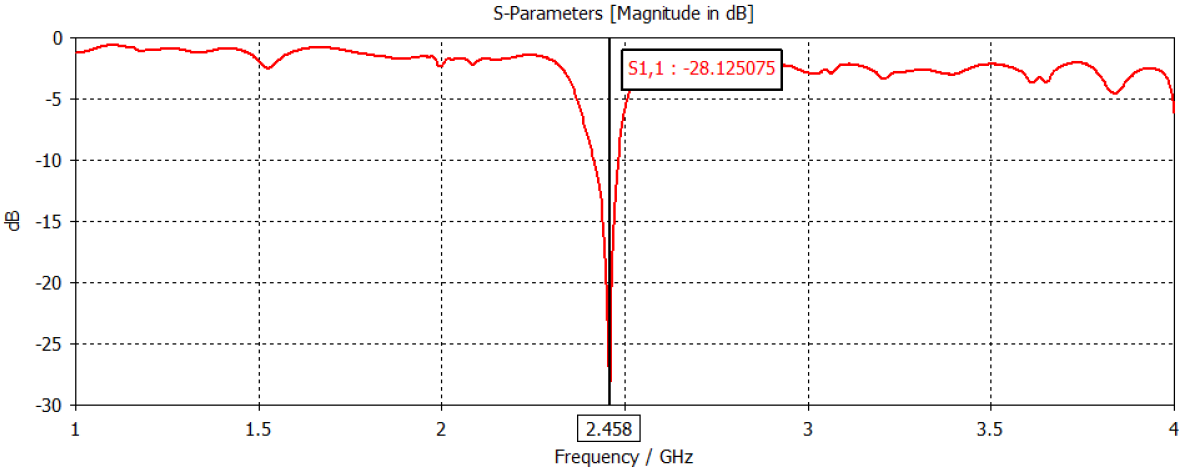


Figure 28: S11 plot of the ultimate patch antenna.

The antenna polar plot is depicted in Figure 29. The obtained gain is about 21 dBi and the side lobe level is -12.5 dB, indicating that the antenna is highly directive in the broadside direction.

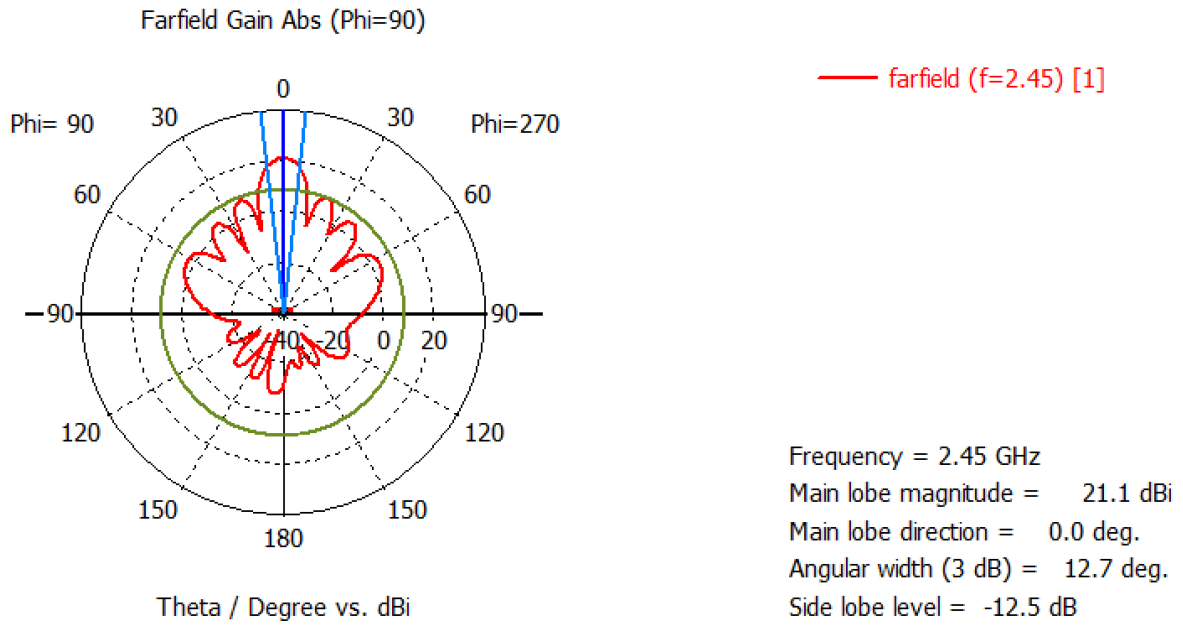


Figure 29: Polar plot of the design.

Some important dimensions are indicated in Figure 30 and the corresponding numerical values are listed in Table 2.

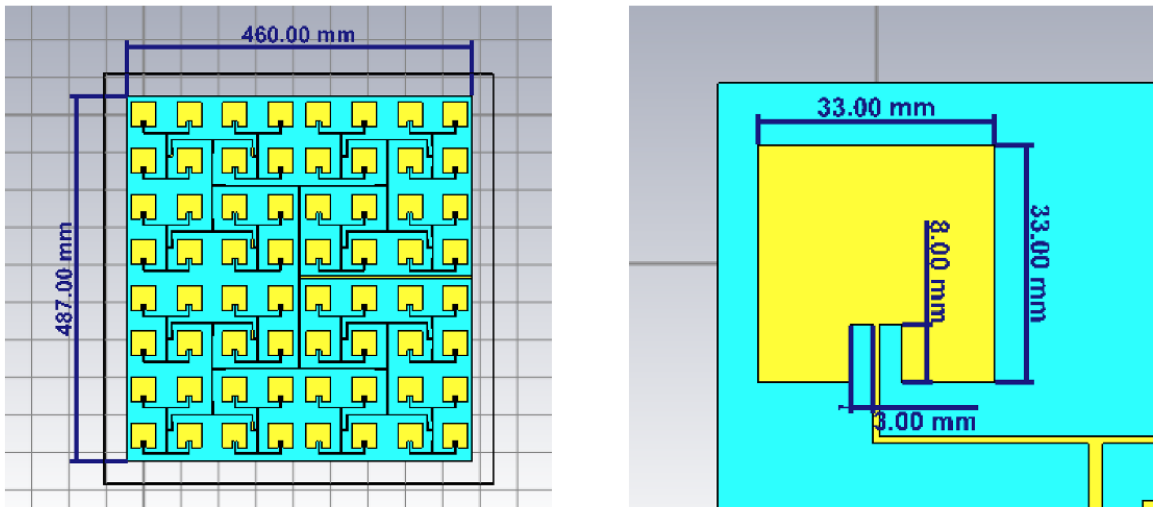


Figure 30: Dimension specifications of the ultimate design.

The antenna feeding line is designed to have an impedance of 100Ω to easily build the array feeding line structure. A quarter-wavelength transformer made by a 70Ω impedance line is used to transform a 50Ω line, made by the parallel of 2 100Ω ones, into a 100Ω . By doing this, we have avoided having quite small value of resistance line at the end. For the last connection, quarter-wave transformer has not used so that we have obtained 50Ω line for the port which is the most common resistance line value.

| Name | Value (mm) |
|----------------------------|-------------------|
| Substrate width | 460.0 |
| Substrate length | 487.0 |
| Substrate thickness | 1.524 |
| Patch thickness | 0.035 |
| Width of 50 Ω line | 3.5 |
| Width of 70 Ω line | 2.0 |
| Width of 100 Ω line | 1.0 |

Table 2: Parameter list.

The design of this 64-patch antenna array concludes the antenna investigations. The antenna gain performance will be evaluated in the power budget chapter. Until there, the components of circuitry (power splitter, rectifier and cable), which are going to be placed on the top layer of the antenna.

4 Circuitry Design

4.1 Power Splitter

Power splitters (also power dividers) couple a defined amount of the electromagnetic power in a transmission line to a port enabling the signal to be used in another circuit. The most basic form of a power splitter is a simple "T" connection, which has one input and two outputs. If the "T" is mechanically symmetrical, a signal applied to the input will be divided into two output signals, equal in amplitude and phase.

Power dividers are subdivided by realization into types: resistive, transmission line (TL), coupled lines, lumped element and mixed structures. The simplest power divider is resistive; unfortunately it possesses more losses than the other types. Transmission line splitters are easy to realize using different technologies, but require a space. Lumped element structures represent equivalent circuits of the transmission line dividers and their characteristics are pared-down. Also when working at RF (2.45 GHz) using a lumped element as power splitter may introduce losses due to the components themselves. The advantage of a splitter using coupled lines refers to the ability of controlling the working bandwidth by varying of the circuit parameters [25].

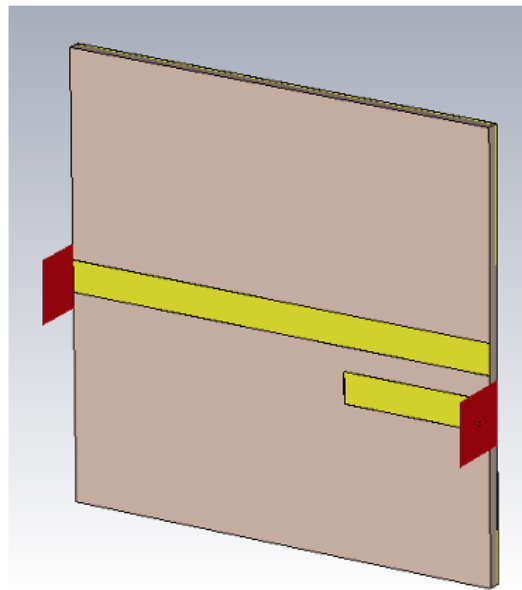


Figure 31: Idea of coupled-line power divider.

Mainly because of its easy configurable feature, we have decided to implement a coupled-line power divider as illustrated in Figure 31. Also, since we consider to have an antenna array, we expected to have a space to fit the coupled-line power divider and rectifier component as well. As shown in Figure 32, we have enough space for the power

splitter and the rectifier. Although the symmetry would be disturbed and there could be some electromagnetic coupling between the power splitter components and the antenna elements, it is expected that the benefit would exceed the drawback and the ultimate results have confirmed it.

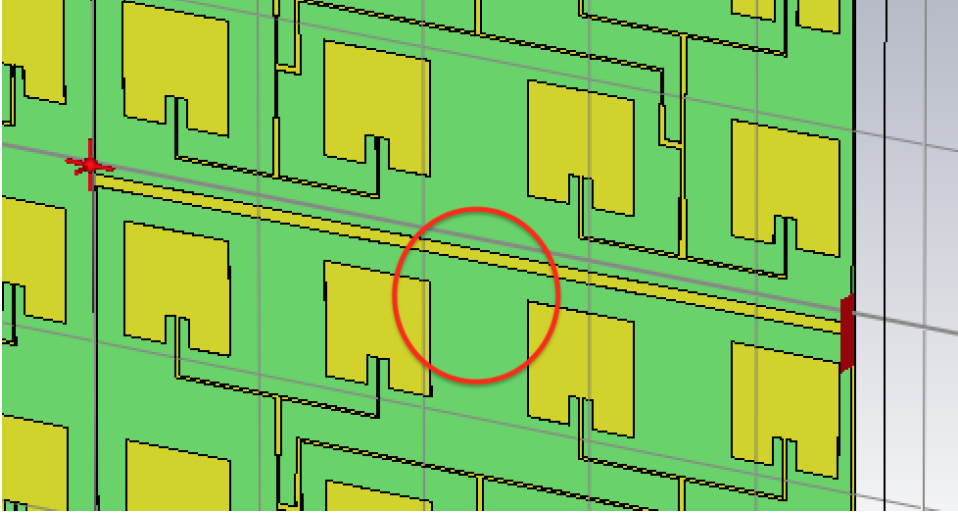


Figure 32: Considered location of the divider.

In order to simulate the performance of the coupled line divider, the schematic that is shown in Figure 33 has been constructed on PathWave Advanced Design System (ADS) which is an electronic design automation software for RF, microwave and signal-integrity applications. By changing width and length of the coupled lines, we can control the ratio of power division. Instead of doing manually, the optimization tool of the software has been used to quickly derive more accurate results. Note that the first analysis has been made using linear simulation but more accurate investigation has been shown using harmonic balance simulation in later.

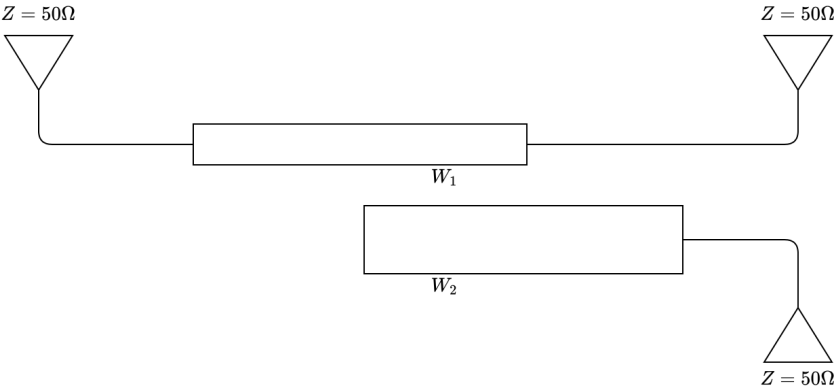


Figure 33: The schematic of the coupled-line power splitter.

At first trials, we have obtained very interesting behavior of the coupled-line power divider as shown in Figure 34. Note that the simulations are made with existence of matching circuit, rectifier and the best load. These parts will be discussed at later stages but it would be beneficial to note at this point that most of the optimization and tuning procedures are made simultaneously. For these purposes, each module is needed to be explained in different chapters.

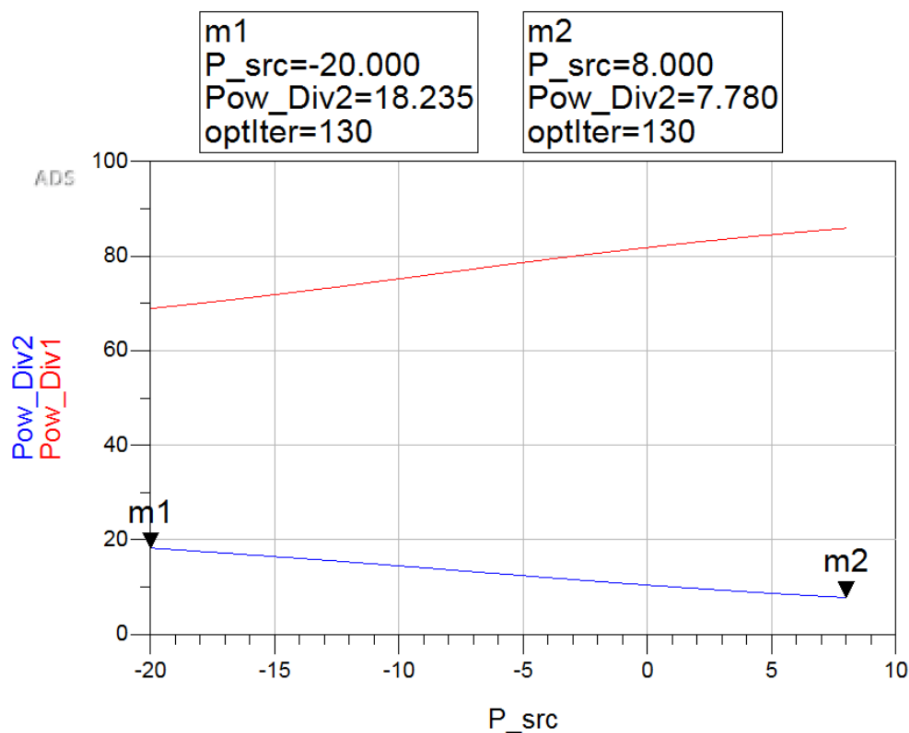


Figure 34: Plot of power division at first trials.

As it can be seen in above figure, the red line represents the power that goes to next transmitting antenna and the blue line is the power that goes into the rectifier and thus to the LoRa node. A preliminary intention has been to design the power splitter to achieve a constant ratio for any received power. However, further analysis have shown how more efficiency on the amount of power that reaches the last tracks can be obtained by considering a variable ratio. In particular for lower input power, low percentages would not be enough to charge the nodes at dedicated time. This concept will be revised again in later stages.

In Figure 35, one can see the power splitter on the antenna board. The thick line is 50Ω line which is connected to coaxial cable and has the bigger portion of the power; the thin line on the left is connected to the rectifier and eventually to the LoRa module. Note also that the thinner line, which is open stub, has been mounted and it is the part of matching circuit between the power splitter and the rectifier. Broader analysis which consists of all circuitry elements has been explained in the next chapter.

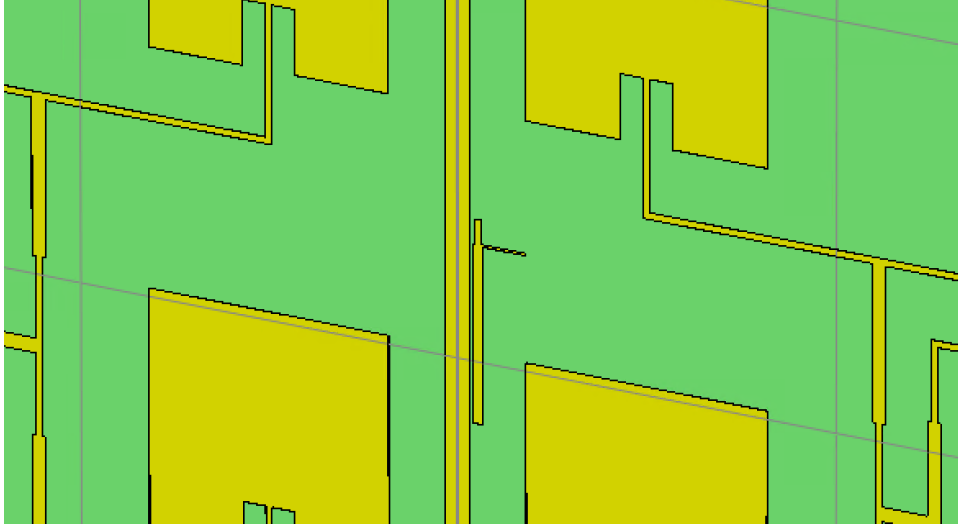


Figure 35: Visualization of the power splitter on the board.

4.2 Rectifier

A rectifier is a non-linear circuit made of one or more diodes that converts alternating current (AC) to direct current (DC). One of the key problems with rectifiers is that AC power has peaks and lows, which may not produce a constant DC voltage. Usually, a smoothing circuit or filter needs to be coupled with the power rectifier to produce a smooth DC current.

Based on the circuit arrangement of the rectifier components, rectifiers are classified into two categories: half-wave rectifier and full-wave rectifier. Half-wave rectifier only converts half of the AC wave into DC signal, whereas full-wave rectifier converts complete AC signal into DC.

The term rectenna is derived from the fact that it is comprised of an antenna coupled with a rectifying circuit. This special type of antenna is used to perform a RF-to-DC power conversion of the signal received by the antenna. During the last four decades, the research on rectenna design has been focused on improving the power conversion efficiency (PCE) and compatibility while reducing the design complexity as well. In general, rectenna applications are likely to be extended up to 20 THz frequencies, but at higher frequencies, sufficient energies are not available in the ambient environment. Therefore, in practice, most of the rectennas are designed to operate in the microwave range of up to 10 GHz [26].

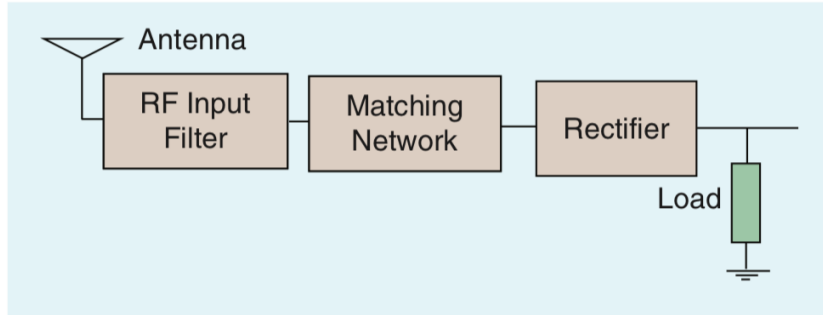


Figure 36: A basic block diagram of a rectenna system [26].

A basic block diagram of a rectenna system is shown in Figure 36. A rectenna system usually comprises an antenna followed by an RF filter, a matching network, and a rectifying circuit. The antenna is used to receive the RF signal, and the rectifying circuit converts this RF signal into the DC signal.

The chosen rectifier topology has been the full-wave one, made by 2 Schottky diodes as illustrated in Figure 37. Schottky diode model is well studied in the literature and it achieves faster switching time, and lower voltage drop which makes it quite adequate for rectifying. In particular, we have used SMS7630 by Skyworks Solutions Inc. since its model is tested in previous projects.

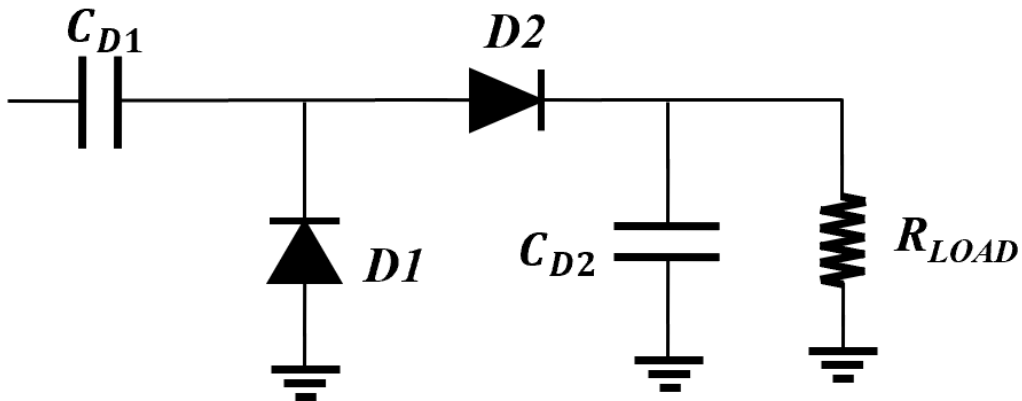


Figure 37: Schematic of the rectifier.

Before placing the actual model for the capacitor, the ideal one is used to optimize the whole rectifier. Once it is determined, the model of capacitor is replaced and a fine tuning of circuit is carried out. The capacitor we have used in this circuit is 22 pF made by Murata Electronics.

The main degree of freedom on this circuit is actually the load. The optimization procedure has been done by indicating a certain threshold for the efficiency and the best possible load value is determined. As a matter of fact, WPT systems use switching converter instead of the load to dynamically track the maximum power point (MPP) condition for any frequency and power level. The MPP tracker is a part of the DC-DC converter and needed to be implemented to the circuit that goes to the LoRa node. However we have used a specific DC-DC converter that allow us to fix a certain load in order to be compliant to our design goals of having a variation on the power splitting. Furthermore, as known the rectifier input impedance also depends on the operating frequency, since this parameter is fixed at 2.45 GHz, the optimization complexity is reduced.

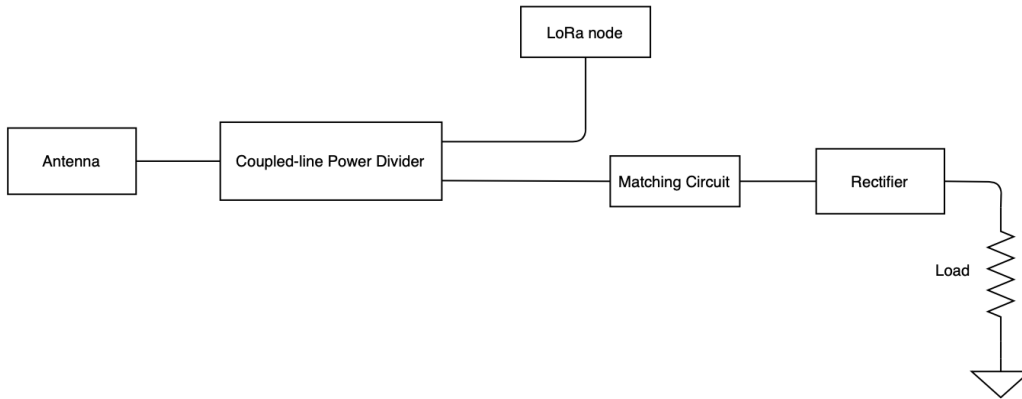


Figure 38: The block diagram of the circuitry analysis.

Figure 38 illustrates the block diagram of the circuitry analysis which has been used to analyze the overall performance. The analysis has been made using harmonic balance method and optimization is made with two goals: power division ratio and rectifier efficiency. As a power input range, we have considered the powers that are from -20 dBm to 8 dBm. Note that the input power we have considered is the power that enters into power splitter, not into rectifier. Below this limit, the input power would be too low to allow a reasonable time for the charging of a LoRa node. Also, having received power level higher than 8 dBm would imply the power transfer at the main track to exceed the European regulation standard (27dBm EIRP).

For the rectification process, we exploit the non-linear region of the I(V) curve of the diode. The non-linearity allows to generate higher harmonics and also DC that would be used to feed our load. Therefore, there is a trade-off between the input signal power and the diode self bias such that the higher the input power, the higher the negative self bias. Because of this, it is expected to have low rectifier efficiency when the input power is low. The optimization goals were set both on achieving the power splitter percentage but also on maximizing the RF-to-DC power conversion efficiency.

As it can be seen in Figure 39, efficiency requirements have been fulfilled and we have obtained a dynamic power ratio behavior from the power splitter. As it mentioned in previous chapters, the dynamic behavior of the divider allows to have higher power levels for lower inputs.

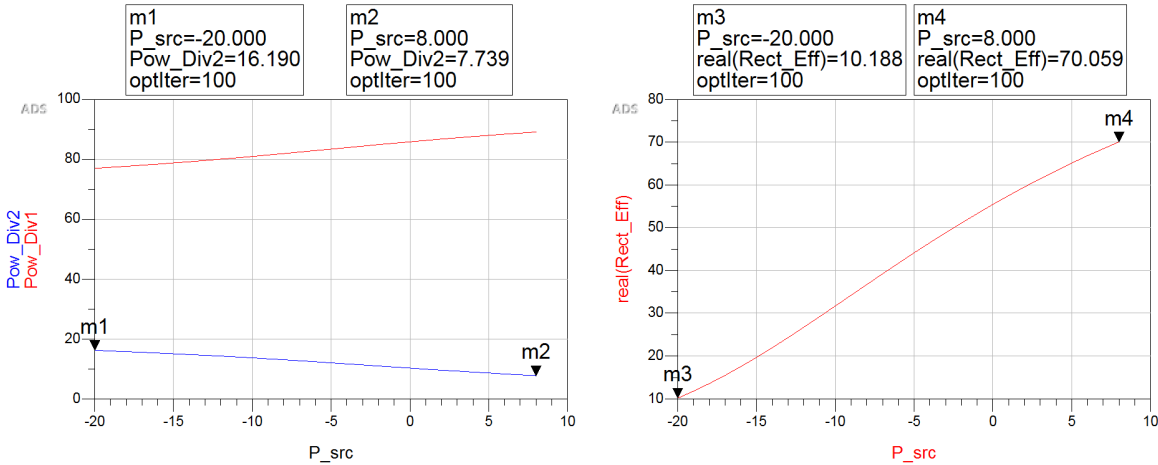


Figure 39: Power division ratio and rectifier efficiency plots.

After a thorough analysis of the circuitry, we have obtained the final overall design as shown in Figure 40. The matching circuit has been designed by means of distributed elements, minimizing the use of lumped ones. The coupled-line power divider geometrical parameters together with the open stub ones have been optimizations variables for matching purposes also.

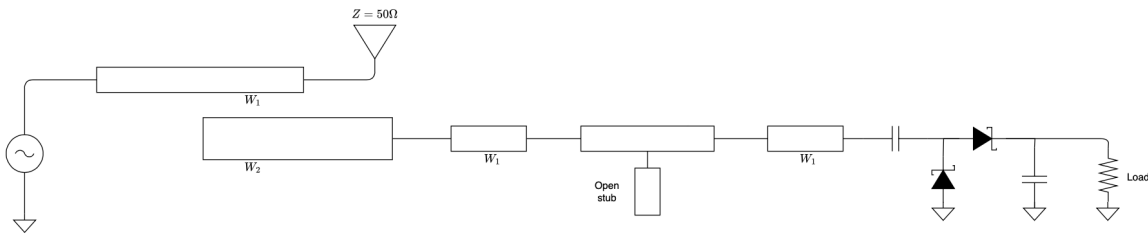


Figure 40: The ultimate schematic of the circuitry design.

The power division and rectifier efficiency of the ultimate design are given in Figure 41. As it can be seen, the input power range has been slightly modified: a -15 dBm has been evaluated as the minimum received power to enable a correct activation and recharge of the LoRa node. Together with the power range variation the optimized power splitting ratio has been changed accounting for a redacted difference between

the percentage between low and high power levels. The rectifier performance is quite adequate for our purpose.

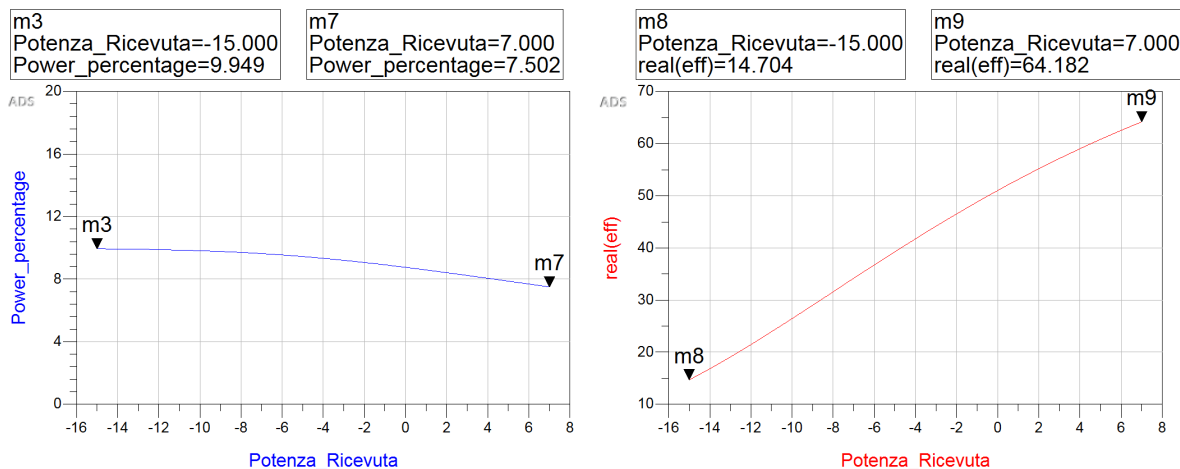


Figure 41: Power division ratio and rectifier efficiency plots of ultimate design.

With this design, we have concluded the part of rectifier. Next chapters describe the choice of the coaxial cable that connects one branch of the power divided to the following transmitting antenna along the carrier.

4.3 Coaxial Cable

Coaxial cable is a type of copper cable built with a metal shield and other components engineered to block signal interference. It includes one physical channel that carries the signal surrounded, after a layer of insulation, by another concentric physical channel, both running along the same axis. The outer channel serves as a ground. Many of these cables or pairs of coaxial tubes can be placed in a single outer sheathing and, with repeaters, can carry information for a great distance. Cable cutaway visualization is shown in Figure 42.

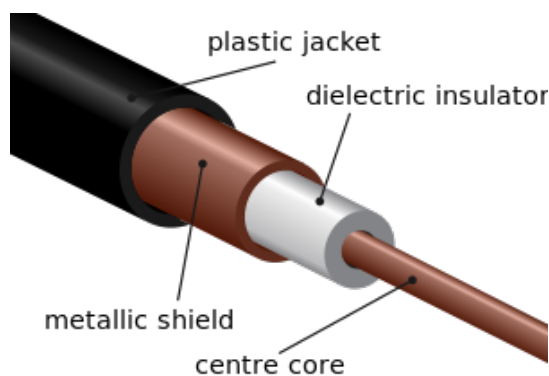



Figure 42: Coaxial cable cutaway [27].

The coaxial cable losses tends to increase proportionally to the increase of the working frequency. Figure 43 shows the characteristics of one the most performing coaxial cables selected from an Italian company. Therefore this also confirms that eliminating 5.8 GHz at the beginning was a good choice.

 Data una potenza immessa di valore X (qualsiasi valore espresso in Watt), la potenza effettiva in uscita dal cavo, viene riportata in tabella sottoforma di percentuale residua.
Se per esempio utilizziamo un cavo come il M&P-ULTRAFLEX 13, immettendo 1000 Watt su una lunghezza di 35m, alla frequenza di 144 MHz, ci rimane il 74.4 % di 1000. Per la potenza massima applicabile, fare riferimento alla Power Handling del cavo in oggetto. Da questi valori sono già stati dedotti i valori di SRL caratteristici di ciascun nostro modello per le rispettive frequenze.

| | | M&P-ULTRAFLEX 13 / .500" | | | | | | | | | | | | | | |
|-------------------------|---------|--------------------------|------|------|------|------|-------|------|------|------|-------|-------|-------|-------|------|---|
| length --> | | 16,4 | 32,8 | 49,2 | 65,6 | 82 | 114,8 | 164 | 246 | 328 | 426,5 | 524,9 | 656,2 | 984,2 | feet | |
| Wave length | | MHz | 5 | 10 | 15 | 20 | 25 | 35 | 50 | 75 | 100 | 130 | 160 | 200 | 300 | m |
| Frequencies / Frequenze | 85.71 m | 3,5 | 99,1 | 98,3 | 97,6 | 96,8 | 96,1 | 94,6 | 92,4 | 88,8 | 85,4 | 81,5 | 77,7 | 73,0 | 62,4 | Useful signal output (residual power %) |
| | 42.85 m | 7 | 98,9 | 97,9 | 96,9 | 95,9 | 94,9 | 93,0 | 90,2 | 85,7 | 81,4 | 76,5 | 71,9 | 66,3 | 54,0 | |
| | 21.42 m | 14 | 98,6 | 97,3 | 96,0 | 94,7 | 93,5 | 91,0 | 87,5 | 81,9 | 76,6 | 70,8 | 65,4 | 58,8 | 45,1 | |
| | 10.71 m | 28 | 98,1 | 96,4 | 94,7 | 93,0 | 91,4 | 88,2 | 83,6 | 76,4 | 69,9 | 62,8 | 56,4 | 48,9 | 34,2 | |
| | 6 m | 50 | 97,6 | 95,4 | 93,2 | 91,1 | 89,0 | 85,0 | 79,3 | 70,7 | 63,0 | 54,9 | 47,8 | 39,7 | 25,0 | |
| | 2 m | 144 | 95,8 | 91,8 | 88,1 | 84,4 | 80,9 | 74,4 | 65,6 | 53,1 | 43,1 | 33,4 | 26,0 | 18,5 | 7,9 | |
| | 69 cm | 430 | 92,7 | 86,0 | 79,9 | 74,1 | 68,8 | 59,3 | 47,4 | 32,7 | 22,5 | 14,3 | 9,1 | 5,0 | | |
| | 23.1 cm | 1296 | 86,5 | 75,2 | 65,4 | 56,9 | 49,5 | 37,4 | 24,5 | 12,0 | 5,7 | | | | | |
| | 12.5 cm | 2400 | 81,2 | 66,4 | 54,2 | 44,2 | 36,1 | 24,0 | 12,9 | 4,3 | | | | | | |
| | 10 cm | 3000 | 78,6 | 62,4 | 49,5 | 39,2 | 31,0 | 19,3 | 9,2 | | | | | | | |
| | 7.5 cm | 4000 | 75,2 | 57,1 | 43,3 | 32,7 | 24,7 | 13,9 | 5,6 | | | | | | | |
| | 6 cm | 5000 | 72,4 | 52,8 | 38,5 | 28,0 | 20,3 | 10,4 | 3,5 | | | | | | | |
| | 5 cm | 6000 | 69,1 | 48,4 | 33,7 | 23,4 | 16,1 | 7,2 | | | | | | | | |
| | 3.75 cm | 8000 | 64,6 | 42,2 | 27,4 | 17,6 | 11,1 | 4,0 | | | | | | | | |
| | 3 cm | 10.000 | 58,7 | 35,1 | 20,5 | 11,5 | 5,9 | | | | | | | | | |
| 2.5 cm | 12.000 | 54,8 | 30,5 | 16,4 | 8,2 | 3,4 | | | | | | | | | | |

M&P-ULTRAFLEX 13 / .500" Power Handling/Temperature (in Continuous Carrier)

Figure 43: Characteristic of a coaxial cable by "Messi & Paoloni" [28].

Assuming the industrial charter that we will used for our model is 20 meters, useful signal output would correspond to 44.2% which will be used at power budget evaluation stage.

5 Power Budget Evaluation

Power penalty or loss budget is an important consideration, since it is an essential requirement that the power is able to be transferred from the main charter to the others and still retain a healthy margin of power strength. It is a well-known fact that every component either active or passive has a power loss associated with it. Similarly there are many losses associated with the transfer link like free space loss, splitter loss, coupler loss and material loss that have to be considered before and after designing the main setup.

In order to construct a model of our system, there are some considerations and loss calculations need to be conducted. We have assumed that the distance that the power will be transferred or, in other words, the distance between the consecutive charters is one meter. Through that, we have calculated the free-space loss using the formula below.

$$FSPL[dB] = 20\log_{10}\left(\frac{4\pi df}{c}\right) \quad (3)$$

where d is the distance, f is the frequency and c is the light of speed. The free-space path loss (FSPL) that we found is 40.23 dB. On the other hand, we have also chosen an appropriate coaxial cable for 2.45 GHz from the above-mentioned company. In our situation, we have assumed that the length of the charter is 20 meters so that we have chosen 20 m of coaxial cable and the cable loss for this distance is given as 3.36 dB.

| | | | | | |
|------------------------------------|--------------|--|--|-------------------------------|--|
| EIRP [dBm] | 27 | | | Main car | |
| Antenna Gain [dBi] | 21 | | | Space between charters | |
| Cable Loss (20m) [dB] | 3.36 | | | Charter | |
| Space Between Charters [m] | 1 | | | | |
| LoRa Energy Need [mJ] | 1.7 | | | | |
| Free Space Attenuation [dB] | 40.23 | | | | |

Figure 44: Dynamic table specification section.

Furthermore, we have constructed a "Dynamic Table" as we call it in order to evaluate the power budget. Figure 44 shows the specification section of the table. This section allow to change some parameters and the evaluation table changes accordingly. As one can see, the variables that we have found has been inserted. The patch antenna array that we have designed had approximately 21 dBi antenna gain and we have assumed that LoRa node would need 1.7 mJ of energy to send basic identification and location information.

We have assumed two different cases mainly because of the different EIRP regulations in Europe (ETSI) and U.S. (FCC). One can enter EIRP as 27 dBm for Europe and 36 dBm for U.S.. This power has been given by the main charter which has actual energy source.

| | | 1 | 2 | 3 |
|------------------------------|--|-------|-------|-------|
| Received Power [dBm] | | 7.77 | 5.85 | 3.91 |
| Received Power [mW] | | 5.991 | 3.847 | 2.462 |
| Power Divider [%] | | 7.5 | 7.8 | 8.1 |
| Power to LoRa Branch [dBm] | | -3.47 | -5.23 | -7.00 |
| Power to LoRa Branch [mW] | | 0.449 | 0.300 | 0.199 |
| Rectification Efficiency [%] | | 65.0 | 59.3 | 53.6 |
| Rectified Power to LoRa [uW] | | 292.1 | 177.9 | 106.9 |
| Charging Time of LoRa [s] | | 5.8 | 9.6 | 15.9 |
| Remaining Power [mW] | | 5.542 | 3.547 | 2.263 |
| Remaining Power [dBm] | | 7.44 | 5.50 | 3.55 |
| Transmitted Power [dBm] | | 4.08 | 2.14 | 0.19 |

Figure 45: Dynamic table charters 1-3.

The dynamic table has been constructed as in Figure 45. The indications with black color, power division ratio and rectifier efficiency percentage, must be filled manually by looking into the results in Figure 41. All the tables that are shown in this chapter have already been filled with the ultimate results. The figure of merit in our case is the charging time of LoRa and it is calculated by dividing LoRa energy need to the rectified power.

| | 4 | 5 | 6 | 7 |
|------------------------------|-------|--------|--------|--------|
| Received Power [dBm] | 1.96 | 0.00 | -1.97 | -3.95 |
| Received Power [mW] | 1.571 | 1.000 | 0.635 | 0.403 |
| Power Divider [%] | 8.3 | 8.5 | 8.7 | 8.9 |
| Power to LoRa Branch [dBm] | -8.85 | -10.71 | -12.58 | -14.46 |
| Power to LoRa Branch [mW] | 0.130 | 0.085 | 0.055 | 0.036 |
| Rectification Efficiency [%] | 50.2 | 47.8 | 43.9 | 40.1 |
| Rectified Power to LoRa [uW] | 65.5 | 40.6 | 24.3 | 14.4 |
| Charging Time of LoRa [s] | 26.0 | 41.8 | 70.1 | 118.3 |
| Remaining Power [mW] | 1.441 | 0.915 | 0.580 | 0.367 |
| Remaining Power [dBm] | 1.59 | -0.39 | -2.37 | -4.36 |
| Transmitted Power [dBm] | -1.77 | -3.75 | -5.73 | -7.72 |

Figure 46: Dynamic table charters 4-7.

By looking at Figure 47, we can say that 11th charter charging time corresponds to approximately 18 minutes. The next charter would definitely need more than 30 minutes to charge and it is not acceptable under our criteria. Therefore, we can conclude that we can charge 11 charters with this specific model.

| | 8 | 9 | 10 | 11 |
|-------------------------------------|--------|--------|--------|--------|
| Received Power [dBm] | -5.94 | -7.94 | -9.95 | -11.97 |
| Received Power [mW] | 0.255 | 0.161 | 0.101 | 0.064 |
| Power Divider [%] | 9.1 | 9.3 | 9.5 | 9.7 |
| Power to LoRa Branch [dBm] | -16.35 | -18.26 | -20.17 | -22.10 |
| Power to LoRa Branch [mW] | 0.023 | 0.015 | 0.010 | 0.006 |
| Rectification Efficiency [%] | 38.7 | 34.7 | 30.2 | 25.8 |
| Rectified Power to LoRa [uW] | 9.0 | 5.2 | 2.9 | 1.6 |
| Charging Time of LoRa [s] | 189.6 | 327.9 | 585.7 | 1068.7 |
| Remaining Power [mW] | 0.231 | 0.146 | 0.092 | 0.057 |
| Remaining Power [dBm] | -6.36 | -8.36 | -10.38 | -12.41 |
| Transmitted Power [dBm] | -9.72 | -11.72 | -13.74 | -15.77 |

Figure 47: Dynamic table charters 8-11.

If we would consider a case in U.S. with 36 dBm of EIRP, we would, of course, reach higher number of carriers. For any other antenna, power splitter or rectifier designs, corresponding variables can easily be changed and the results will be changed accordingly.

To sum up, we have constructed a "Dynamic Table" to assess power budget calculation of our system with a particular case. This table allows to find how many carriers can be charged in dedicated time with desired specifications. The calculation elements can be adjusted conveniently and the updated results are dynamically given on the table.

6 Conclusion

Information and communication technologies are fundamental in the development of Smart City and Smart Mobility concepts. In particular, wireless sensor networks are essential for these services as they offer very low cost of deployment, low power consumption and maintenance cost. Long range capability of the nodes allows deployment at remote locations. Local RF technologies including Bluetooth and Wi-Fi, do not meet the range requirements to support these kind of applications.

In this thesis, we addressed the problem of powering wireless sensor nodes of a tracking system in industrial plants. The localization and tracking system we have considered uses LoRa which is a communication technology with low power consumption, long distance, low cost and easy deployment. One of the main contributions of our work is a complete wireless power transfer model that indicates the charging time of LoRa nodes at each charter.

The system is designed to have antennas on the front and back of the charters such that a power splitter on one of which divide certain portion of the power and a rectifier converts this power into DC for the LoRa modules. The other big portion has been connected to the other transmitting antenna by coaxial cables. It is our main intention to design an efficient battery-less tracking system for industrial charters. This contribution can certainly be exploited to solve battery problem of low-power consumption wireless sensor nodes in the industry.

Different types of antenna designs have been presented in this thesis. First, a monopole antenna array has been investigated with relatively low cost dielectric material. Although the performance has given good results, the presence of a back plane to reflect back radiation makes this design problematic to realize in our scenario. Second, a patch antenna array has been designed using more robust substrate and its performance was quite effective. At the end, the design of 64-patch antenna array with antenna gain of 21 dBi was decided for the ultimate model.

Besides proposing various antenna types, choosing the operating frequency was another dilemma. Three different frequencies have been investigated; 868 MHz, 2.45 GHz and 5.8 GHz. The lowest and the highest frequencies are eliminated because of large antenna size and high loss, respectively. Since this elimination has been done in early stages, the through check of different topologies have been conducted with the optimum frequency, 2.45 GHz.

Moreover, a discussion on different representations of circuitry analysis has been provided. This module mainly consists of power splitter and rectifier. The simulations that we have performed show that we have obtained a coupled-line power splitter with

dynamic power ratio which allows to have more power outcome for lower input power levels. Also, a full-wave rectifier has been designed using Schottky diodes which achieves faster switching time, and lower voltage drop.

The main focus of our thesis was to power as many LoRa nodes as possible. To do that, a through evaluation of power budget has been made by calculation all type of gains and losses. Our contribution is creating a dynamic table that shows charging time of LoRa nodes and it changes according to some input values that a user can insert. For a certain limitation of charging, one can easily see the amount of charters that can be charged by looking at this table.

The final results show that our approach obtains both sufficient and efficient battery-less solution for wireless system of localization and tracking the industrial carriers.

7 Future Work

Many different adaptations, tests, and measurements have been left for the future due to lack of time and resources. Future work concerns deeper analysis of particular mechanisms, new proposals to try different methods, or simply curiosity.

In particular, it had been planned to construct a prototype to make some measurements. The prototype is under construction and measurement are scheduled in the next future. Due to order delays, the prototype could not be ready to complete some experiments and cannot be added into this thesis work.

8 Bibliography

- [1] C. Stewart, C. Luebkehan, M. Morrell, and L. Goulding, “Future of Rail 2050”, Arup, Technical Report, 2014. [Online]. Available: <https://www.arup.com/perspectives/publications/research/section/future-of-rail-2050>.
- [2] R. Cruz, J. Jardim, J. Mira, and C. Teixeira, “Smart rail for smart mobility,” in *2018 16th International Conference on Intelligent Transportation Systems Telecommunications (ITST)*, 2018, pp. 1–7.
- [3] H. Dia, “The real-time city: Unlocking the potential of smart mobility,” in *Proceedings of the Australasian Transport Research Forum 2016*, 2016. [Online]. Available: <https://www.australasiantransportresearchforum.org.au/sites/default/files/ATRF2016-Full-papers-resubmission-189.pdf>.
- [4] J. Liu, K. Xiong, P. Fan, and Z. Zhong, “Rf energy harvesting wireless powered sensor networks for smart cities,” *IEEE Access*, vol. 5, pp. 9348–9358, 2017.
- [5] M. Gao, P. Wang, Y. Wang, and L. Yao, “Self-powered zigbee wireless sensor nodes for railway condition monitoring,” *IEEE Transactions on Intelligent Transportation Systems*, vol. 19, no. 3, pp. 900–909, 2018.
- [6] F. Righetti, C. Vallati, G. Anastasi, G. Masetti, and F. di Giandomenico, “Failure management strategies for iot-based railways systems,” in *2020 IEEE International Conference on Smart Computing (SMARTCOMP)*, 2020, pp. 386–391.
- [7] B. Ai, A. F. Molisch, M. Rupp, and Z.-D. Zhong, “5g key technologies for smart railways,” *Proceedings of the IEEE*, vol. 108, no. 6, pp. 856–893, 2020.
- [8] B. Ai, X. Cheng, T. Kürner, Z.-D. Zhong, K. Guan, R.-S. He, L. Xiong, D. W. Matolak, D. G. Michelson, and C. Briso-Rodriguez, “Challenges toward wireless communications for high-speed railway,” *IEEE Transactions on Intelligent Transportation Systems*, vol. 15, no. 5, pp. 2143–2158, 2014.
- [9] Z. Li, X. Li, G. Mou, D. Jiang, X. Bao, and Y. Wang, “Design of localization system based on ultra-wideband and long range wireless,” in *2019 IEEE 11th International Conference on Advanced Infocomm Technology (ICAIT)*, 2019, pp. 142–146.
- [10] A. Costanzo, D. Dardari, J. Aleksandravicius, N. Decarli, M. Del Prete, D. Fabbrì, M. Fantuzzi, A. Guerra, D. Masotti, M. Pizzotti, and A. Romani, “Energy autonomous uwb localization,” *IEEE Journal of Radio Frequency Identification*, vol. 1, no. 3, pp. 228–244, 2017.

- [11] G. Paolini, D. Masotti, M. Guermandi, M. Shanawani, L. Benini, and A. Costanzo, “An ambient-insensitive battery-less wireless node for simultaneous powering and communication,” in *2020 50th European Microwave Conference (EuMC)*, 2021, pp. 522–525.
- [12] L. Li, J. Ren, and Q. Zhu, “On the application of lora lpwan technology in sailing monitoring system,” in *2017 13th Annual Conference on Wireless On-demand Network Systems and Services (WONS)*, 2017, pp. 77–80.
- [13] F. Flammini, A. Gaglione, D. Tokody, and D. Dohrilovic, “Lora wan roaming for intelligent shipment tracking,” in *2020 IEEE Global Conference on Artificial Intelligence and Internet of Things (GCAIoT)*, 2020, pp. 01–02.
- [14] I. F. Priyanta, F. Golatowski, T. Schulz, and D. Timmermann, “Evaluation of lora technology for vehicle and asset tracking in smart harbors,” in *IECON 2019 - 45th Annual Conference of the IEEE Industrial Electronics Society*, vol. 1, 2019, pp. 4221–4228.
- [15] Martin Keenan, “How wireless power transfer can help make the world’s lithium go further”, September 19, 2017. [Online]. Available: <https://www.avnet.com/wps/portal/abacus/resources/article/wireless-power-transfer/>.
- [16] U. Guler, M. S. Sendi, and M. Ghovanloo, “A dual-mode passive rectifier for wide-range input power flow,” in *2017 IEEE 60th International Midwest Symposium on Circuits and Systems (MWSCAS)*, 2017, pp. 1376–1379.
- [17] H. Ma, Y. J. Gao, Q. Yang, J. X. Tao, and Z. Ji, “Foggy distance warning system based on lora technology,” in *2021 International Conference on Intelligent Transportation, Big Data Smart City (ICITBS)*, 2021, pp. 550–553.
- [18] S. Sağır, Kaya, C. Şişman, Y. Baltacı, and S. Ünal, “Evaluation of low-power long distance radio communication in urban areas: Lora and impact of spreading factor,” in *2019 Seventh International Conference on Digital Information Processing and Communications (ICDIPC)*, 2019, pp. 68–71.
- [19] O. Georgiou and U. Raza, “Low power wide area network analysis: Can lora scale?” *IEEE Wireless Communications Letters*, vol. 6, no. 2, pp. 162–165, 2017.
- [20] A technical overview of LoRa and LoRaWaN, LoRa Alliance, November 2015.
- [21] Lora-alliance.org, Available: <https://lora-alliance.org/about-lorawan>.

- [22] M. Aref and A. Sikora, "Free space range measurements with semtech lora™ technology," in *2014 2nd International Symposium on Wireless Systems within the Conferences on Intelligent Data Acquisition and Advanced Computing Systems*, 2014, pp. 19–23.
- [23] B. Kim and K.-i. Hwang, "Cooperative downlink listening for low-power long-range wide-area network," *Sustainability*, vol. 9, no. 4, 2017. [Online]. Available: <https://www.mdpi.com/2071-1050/9/4/627>
- [24] R. Gonalves, P. Pinho and N. B. Carvalho, "Compact Frequency Reconfigurable Printed Monopole Antenna", *International Journal of Antennas and Propagation*, vol. 2012, pp. 6.
- [25] R. Kravchenko, M. Stadler, and E. Leitgeb, "A new uwb coupled transmission line power divider," in *2010 IEEE MTT-S International Microwave Symposium*, 2010, pp. 1568–1571.
- [26] D. Surender, T. Khan, F. A. Talukdar, and Y. M. Antar, "Rectenna design and development strategies for wireless applications: A review," *IEEE Antennas and Propagation Magazine*, pp. 2–15, 2021.
- [27] Coaxial cable From Wikipedia, the free encyclopedia, Available: <https://en.wikipedia.org/wiki/Coaxial-cable>.
- [28] Messi & Paoloni, Available: <https://messi.it/en/comparison-chart-attenuationpower-ratio.htm>.